AGU PUBLICATIONS

Tectonics

RESEARCH ARTICLE
10.1002/2016TC004229

Key Points:
- A releasing fault bend formed along the ASRR during left-lateral shearing, changing to a restraining bend after right-lateral reactivation
- The Ailao Shan Shear Zone experienced two phases of rapid exhumation in the Miocene
- The second cooling phase possibly reflects renewed plateau growth associated with lower crustal flow

Supporting Information:
- Supporting Information S1

Correspondence to:
B. Zhang,
geozhangbo@pku.edu.cn

Citation:
Wang, Y., B. Zhang, L. M. Schoenbohm, J. Zhang, R. Zhou, J. Hou, and S. Ai (2016), Late Cenozoic tectonic evolution of the Ailao Shan-Red River fault (SE Tibet): Implications for kinematic change during plateau growth, *Tectonics*, *35*, 1969–1988, doi:10.1002/2016TC004229.

Received 8 MAY 2016
Accepted 18 JUL 2016
Accepted article online 25 JUL 2016
Published online 30 AUG 2016

Late Cenozoic tectonic evolution of the Ailao Shan-Red River fault (SE Tibet): Implications for kinematic change during plateau growth

Yang Wang[1,2], Bo Zhang[1], Lindsay M. Schoenbohm[2], Jinjiang Zhang[1], Renjie Zhou[3], Jianjun Hou[1], and Sheng Ai[1]

[1]The Key Laboratory of Orogenic Belts and Crustal Evolution, School of Earth and Space Sciences, Peking University, Beijing, China, [2]Department Earth Sciences, University of Toronto, Toronto, Ontario, Canada, [3]School of Geography, Planning and Environmental Management, University of Queensland, Brisbane, Queensland, Australia

Abstract Surface uplift, river incision, shear zone exhumation, and displacement along active faults have all interacted to shape the modern landscape in the southeastern margin of the Tibetan Plateau. The Ailao Shan-Red River fault, a major structure in the tectonic evolution of southeastern Asia, is an excellent recorder of these processes. We present new stratigraphic, structural, and low-temperature thermochronologic data to explore its late Cenozoic tectonic and geomorphic evolution. The stratigraphic and structural observations indicate that the major bend in the fault was a releasing bend with significant Miocene sedimentation in the early–middle Miocene but became a restraining bend with abundant shortening structures developed after the late Miocene reversal of displacement. We also document exhumation of the shear zone from two low-temperature thermochronologic transects. New apatite (U-Th)/He(AHe) data and published thermochronologic results reveal two accelerated cooling episodes, backed by stratigraphic and geomorphic observations. The first rapid cooling phase occurred from ca. 27 to 17 Ma with removal of cover rocks and exhumation of the shear zone. The second accelerated cooling episode revealed by our AHe data commenced at 14–13 Ma, lasting 2–3 Myr. The Ailao Shan range may have risen to its modern elevation with high-relief topography developing due to river incision. We interpret the onset of this rapid exhumation to reflect renewed plateau growth associated with lower crustal flow.

1. Introduction

Convergent orogens often experience major changes in kinematics and structural style during later stages of their tectonic evolution, reflecting critical shifts in the dominant dynamic systems. Outstanding examples include the transition from predominantly thrust faulting to strike-slip or normal faulting in the Arabia-Asia collision zone [e.g., *Copley and Jackson*, 2006], the initiation of basin and range extension in western U.S. [e.g., *Sonder et al*., 1987], and the onset of regional surface uplift in the southeastern margin of the Tibetan Plateau [e.g., *Royden et al*., 1997, 2008; *Clark et al*., 2005]. The India-Eurasia continental collision has created the Tibetan Plateau (Figure 1a), a natural laboratory for us to understand mountain building and plateau growth [e.g., *Molnar and Tapponnier*, 1975; *Tapponnier et al*., 1982, 2001; *Armijo et al*., 1989; *Yin*, 2010]. Models for the evolution of the Tibetan Plateau vary between two members which may not be mutually exclusive: those that emphasize the lateral extrusion of crustal blocks with strain localized along major boundary faults [e.g., *Tapponnier et al*., 1982] and the other points to crustal thickening and diffuse or continuous deformation [e.g., *Houseman and England*, 1993; *Royden et al*., 2008]. Therefore, the continental-scale strike-slip faults in the Tibetan Plateau and its margins have great significance for studying the deformation style and changing kinematics during plateau growth in the context of these models.

The Ailao Shan-Red River fault, which lies in the southeastern margin of the Tibetan Plateau, extends approximately 1000 km from SE Tibet to the South China Sea (Figure 1b). The left-lateral shear zones that make up the Ailao Shan-Red River fault include, from NW to SE, the Xuelong Shan, Diancang Shan, Ailao Shan, and Day Nui Con Voi Shear Zones (Figure 2a), which are interpreted as the northeastern boundary of the Indochina block, accommodating the SE block extrusion in the early stages of collision [e.g., *Tapponnier et al*., 1990; *Leloup et al*., 1995; *Yin and Harrison*, 2000]. Notably, the shear sense reversed in Miocene-Pliocene time, and right-lateral movement occurred on the Red River fault which lies to the NE of and subparallel to the shear zones [e.g., *Allen et al*., 1984; *Replumaz et al*., 2001; *Schoenbohm et al*., 2006a]. The reason for

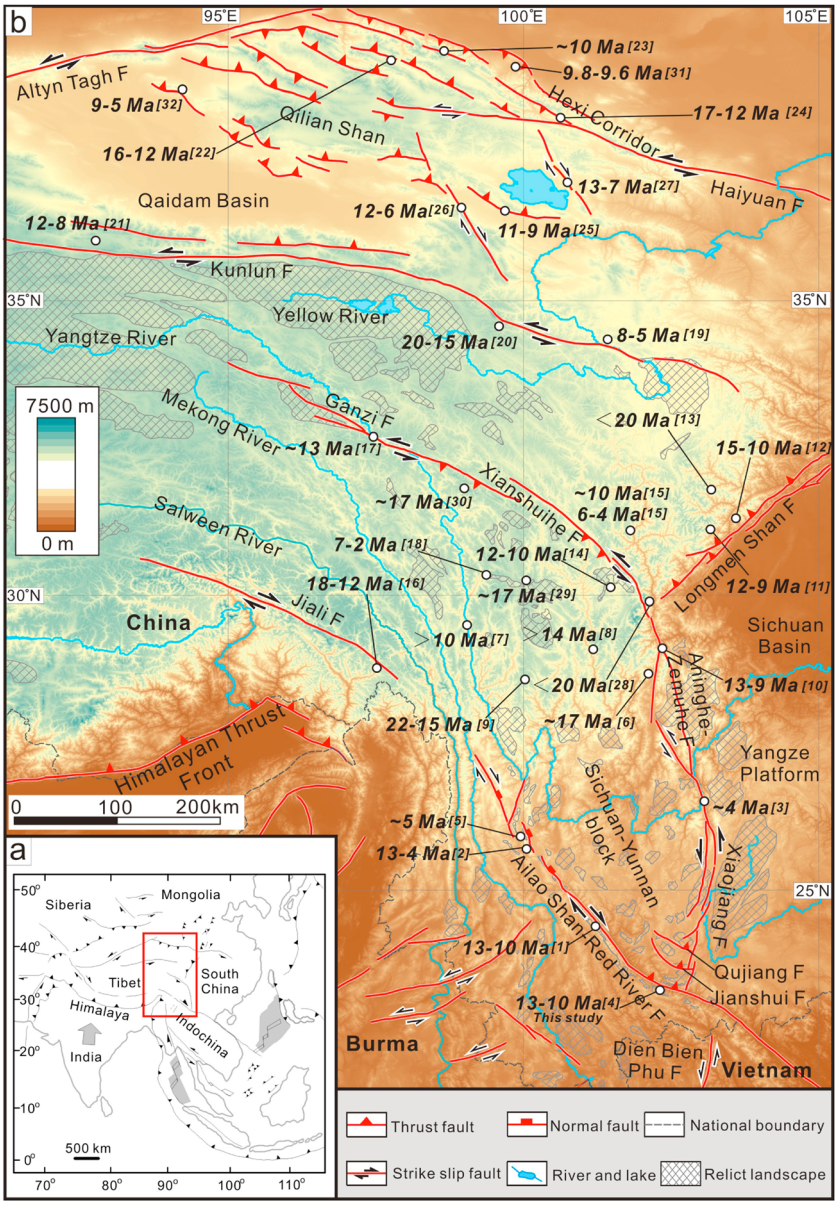

Figure 1. (a) Major structures in the Eurasia plate (compiled from *P. L. Wang et al.* [1998], *Tapponnier et al.* [2001], and *Yin* [2010]). The red rectangle indicates Figure 1b. (b) Topography and major faults of the eastern Tibetan Plateau (compiled from *Xu and Deng* [1996], *Tapponnier et al.* [2001], *Shen et al.* [2005], and *Duvall et al.* [2013]). The gray cross-hatched areas are relict landscape (after *Clark et al.* [2006] and *Royden et al.* [2008]). The ages indicate the proposed timing of initiation or accelerated fault movement or bedrock exhumation [*Leloup et al.*, 2001; *Roger et al.*, 1995; *Bergman et al.*, 1997; *E. Wang et al.*, 1998; *Xu and Kamp*, 2000; *Jolivet et al.*, 2001, 2015; *Kirby et al.*, 2002; *Lee et al.*, 2003; *Clark et al.*, 2005; *Reid et al.*, 2005; *Yuan et al.*, 2006, 2011; *Lai et al.*, 2007; *Bovet et al.*, 2009; *Godard et al.*, 2009; *Wang et al.*, 2009; *Ouimet et al.*, 2010; *Zheng et al.*, 2010; *Cao et al.*, 2011; *E. Wang et al.*, 2012; *S. Wang et al.*, 2012; *H. Zhang et al.*, 2012; *Duvall et al.*, 2013; *Fang et al.*, 2013; *Tian et al.*, 2014; *Zhang et al.*, 2015].

the kinematic change in the Ailao Shan-Red River fault is controversial, mainly because its tectonic evolution, particularly after 17 Ma, remains unclear. Previous thermochronologic data broadly suggest the cooling of the entire shear zone from ca. 34 to 17 Ma, putting a constraint on the duration of left-lateral shearing [e.g., *Leloup et al.*, 1995, 2001; *Harrison et al.*, 1996; *P. L. Wang et al.*, 1998; *Gilley et al.*, 2003]. However, there is little data reported for the unroofing history during the middle–late Miocene when a major change in fault kinematics may take place.

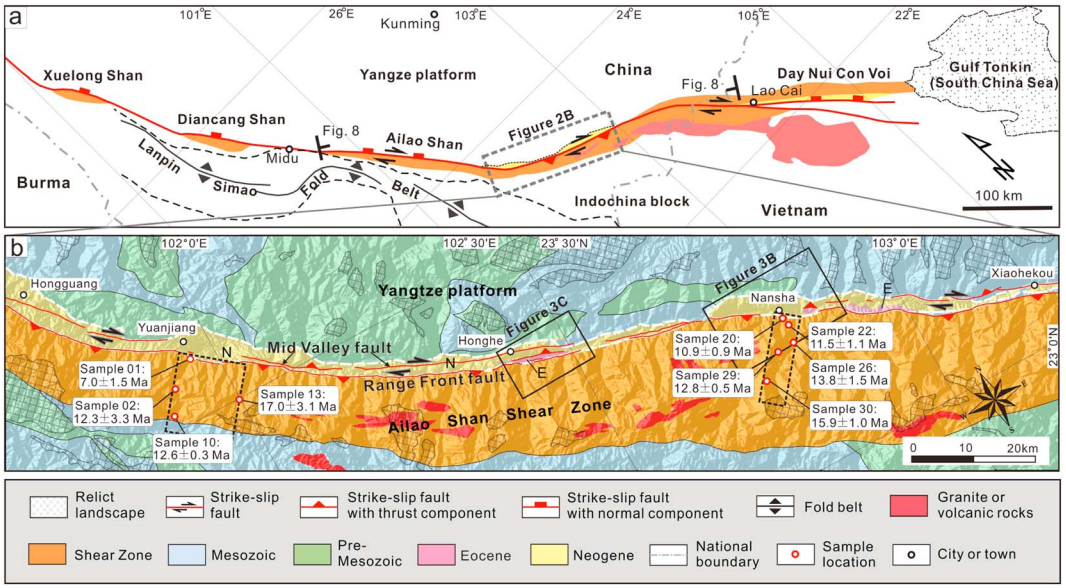

Figure 2. (a) Simplified geologic map of the Ailao Shan-Red River fault (after *Harrison et al.* [1996] and *P. L. Wang et al.* [1998]). The left-lateral shear zones that make up the Ailao Shan-Red River fault, including the Xuelong Shan, Diancang Shan, Ailao Shan, and Day Nui Con Voi Shear Zones, extend from SW China, through Vietnam, into the South China Sea. The right-lateral active faults are located on their northeast side. (b) Geologic map of the study area compiled from Geologic Map of Red River Active Fault, scale 1:50,000 [*Guo et al.*, 2013] and *BGMR* [1990]. White dashed lines are the boundary of the Oligocene-Miocene basin in the bend area. The Range Front fault follows the base of the Ailao Shan range. The Mid Valley fault cut through the Oligocene-Miocene strata and Quaternary deposits. Apatite (U-Th)/He samples were collected along two transects across the Ailao Shan Shear Zone. Dashed boxes indicate the swath profile locations of Figures 6a and 6c.

In this study, we report new data from sedimentology, structural geology, and apatite (U-Th)/He (AHe) thermochronology, in order to provide temporal and kinematic constraints on the tectonic and geomorphic evolution of the Ailao Shan-Red River fault. Our AHe data help to reveal the cooling history (<80°C) of the Ailao Shan Shear Zone which was previously poorly constrained. We then discuss the timing and exhumation mechanism of the shear zone, which may relate to broader deformation in the context of models for the growth of the Tibetan Plateau.

2. Geologic Setting

The southeastern margin of the Tibetan Plateau has been extensively deformed as a result of the India-Asia convergence. It is topographically characterized by an elevated, low-relief landscape, which is continuous with the Tibetan Plateau and is deeply incised by the Salween, Mekong, Yangtze, and Red Rivers and their major tributaries (Figure 1b) [e.g., *Schoenbohm et al.*, 2004; *Clark et al.*, 2005; *Liu-Zeng et al.*, 2008; *Yang et al.*, 2016]. The low-relief surface is best preserved on the northern part of the Ailao Shan range and can be traced discontinuously toward the southeast along the range crest [*Schoenbohm et al.*, 2004]. The timing of regional surface uplift remains uncertain despite the decades of studies, ranging from the early Miocene (ca. 20–15 Ma) or even earlier [e.g., *E. Wang et al.*, 2012; *Tian et al.*, 2014; *Li et al.*, 2015] to the late Miocene (<10 Ma) [e.g., *Kirby et al.*, 2002; *Clark et al.*, 2005; *Schoenbohm et al.*, 2006b; *Ouimet et al.*, 2010].

The Ailao Shan Shear Zone, together with Xuelong Shan, Diancang Shan, and Day Nui Con Voi Shear Zones, forms a profound geologic discontinuity, extending from SW China, through Vietnam, and into the South China Sea (Figure 2a) [e.g., *Tapponnier et al.*, 1990]. Metamorphic rocks of the shear zone are amphibolite grade with well-developed, steeply northeast dipping foliation that bears a strong subhorizontal stretching lineation [e.g., *Leloup et al.*, 1995, 2001; *Searle et al.*, 2010]. Peak metamorphic conditions are 550–780°C and 3–7 kbar, indicating that rocks of the shear zone were formed at a depth of approximately 18 km [*Leloup and Kienast*, 1993]. Ductile left-lateral shear sense indicators are well preserved [e.g., *Leloup et al.*, 1995, 2001; *Zhang et al.*, 2006]. The magnitude of offset, difficult to determine due to the lack of well-correlated geologic features, is estimated to be 700 ± 200 km [*Leloup et al.*, 1995, 2001; *Chung et al.*, 1997].

The regional active fault systems in the southeastern margin of the Tibetan Plateau mainly include the Red River fault and the Xianshuihe-Xiaojiang fault system (Figure 1b). The Red River fault lies on the northeast side of the Ailao Shan Shear Zone (Figure 2a). In contrast to the ductile, left-lateral shear zone, the Red River fault is a right-lateral structure. The offset is estimated to be 5.5 to 54 km based on geomorphic and geologic data with slip rates from 2 to 10 mm/yr due to geomorphic ambiguity [*Allen et al*., 1984; *E. Wang et al*., 1998; *Replumaz et al*., 2001; *Schoenbohm et al*., 2006a]; a minor oblique extensional component occurred on the northern part of the fault, which is limited to less than 750 m vertical displacement [*Schoenbohm et al*., 2004]. The north to northwest trending Xianshuihe-Xiaojiang fault system is composed of four segments (from NW to SE): the Ganzi, Xianshuihe, Anninghe-Zemuhe, and Xiaojiang faults (Figure 1b) [*Allen et al*., 1991; *E. Wang et al*., 1998; *Shen et al*., 2003]. It is characterized by left-lateral strike slip with a slip-rate of approximately 10–11 mm/yr along its entire length in the late Quaternary, and it has experienced a 60 km left-lateral displacement from the late Pliocene to early Quaternary [*E. Wang et al*., 1998; *Shen et al*., 2005]. The Sichuan-Yunnan block which is bounded by these two fault systems is moving toward the southeast at a rate of ca. 3 mm/yr and is undergoing clockwise rotation around the eastern Himalayan syntaxis (Figure 1b) [*Xu and Deng*, 1996].

3. Basin Analysis

Bends, en echelon steps, and other irregularities in continental-scale faults can create basins, which in turn record information about the history of faulting. The Ailao Shan-Red River fault strikes N40°–50°W along most of its length but changes to N60°–70°W between the towns of Hongguang and Xiaohekou (Figures 2a and 2b), marking a prominent bend [*E. Wang et al*., 1998]. An Oligocene-Miocene basin, which is approximately 130 km long and 1–4 km wide, developed in the bend area. We present a stratigraphic and structural framework that integrates existing data with our own new observations in order to explore its evolution history.

3.1. Stratigraphy

The Oligocene to Miocene sedimentary strata are well preserved despite being extensively deformed both by structures related to shear zone exhumation and by activity along the Red River fault [*Schoenbohm et al*., 2005]. The stratigraphy places important constraints on the unroofing history of the Ailao Shan Shear Zone and its geomorphic evolution.

3.1.1. Oligocene

Oligocene strata are distributed discontinuously along the entire Red River valley, mainly consisting of gray and purple sandstone, mudstone, laminated gray and white gypsum, and conglomerate. The sandstone and mudstone are highly deformed and weathered. The conglomerate is only locally observed in the upper part of this unit, containing clasts derived from Yangtze platform rocks (Figure 3a); Ailao Shan derived clasts are notably absent. The thickness of the Oligocene strata is unclear since continuously outcropping sections are rare in the Red River valley. A lacustrine origin of this section is inferred based on the fine-grained sediments and evaporite deposits [*Schoenbohm et al*., 2005]. This unit is inferred to be Oligocene in age [e.g., *Bureau of Geology and Mineral Resources of Yunnan Province (BGMR)*, 1990].

3.1.2. Miocene

Miocene strata are continuous between Hongguang and Xiaohekou along the Red River valley with a thickness of approximately 2000 m [*Xiang et al*., 2007]. They rest unconformably upon the Oligocene. Four distinct, conformable units can be identified. We synthesize new observations and existing geochronologic results to complete the Miocene stratigraphic column (Figure 3a). The first three units are given a descriptive name following *Schoenbohm et al*. [2005]; we introduce a new name for the fourth, previously unidentified unit.

The lowest unit of this section is the Limestone Conglomerate [*Schoenbohm et al*., 2005]. Our observations indicate that in the Nansha area (transect a-a′, Figures 3a and 3b) this unit is characterized by poorly sorted, angular to subangular clasts in a fine matrix (Figure 4a). These medium sand to cobble-sized clasts are mainly limestone with a small portion of quartz, which are likely derived from Yangtze platform rocks (Figure 2b). Thin interbedded sandstone is also present. We observed that the Limestone Conglomerate is a mix of poorly sorted and well-rounded sediments with sandstone and limestone clasts at some locations. We document the thickness of this unit to be more than 600 m. Fossils previously collected from the Limestone Conglomerate in the southeast of Yuanjiang are Miocene in age [*Schoenbohm et al*., 2005]. Samples collected at the base of those strata yield apatite fission-track (AFT) dates of 20.7 ± 2.4 Ma and 20.8 ± 7.8 Ma, providing a maximum age for the unit (Figure 3a) [*Xiang et al*., 2006, 2007].

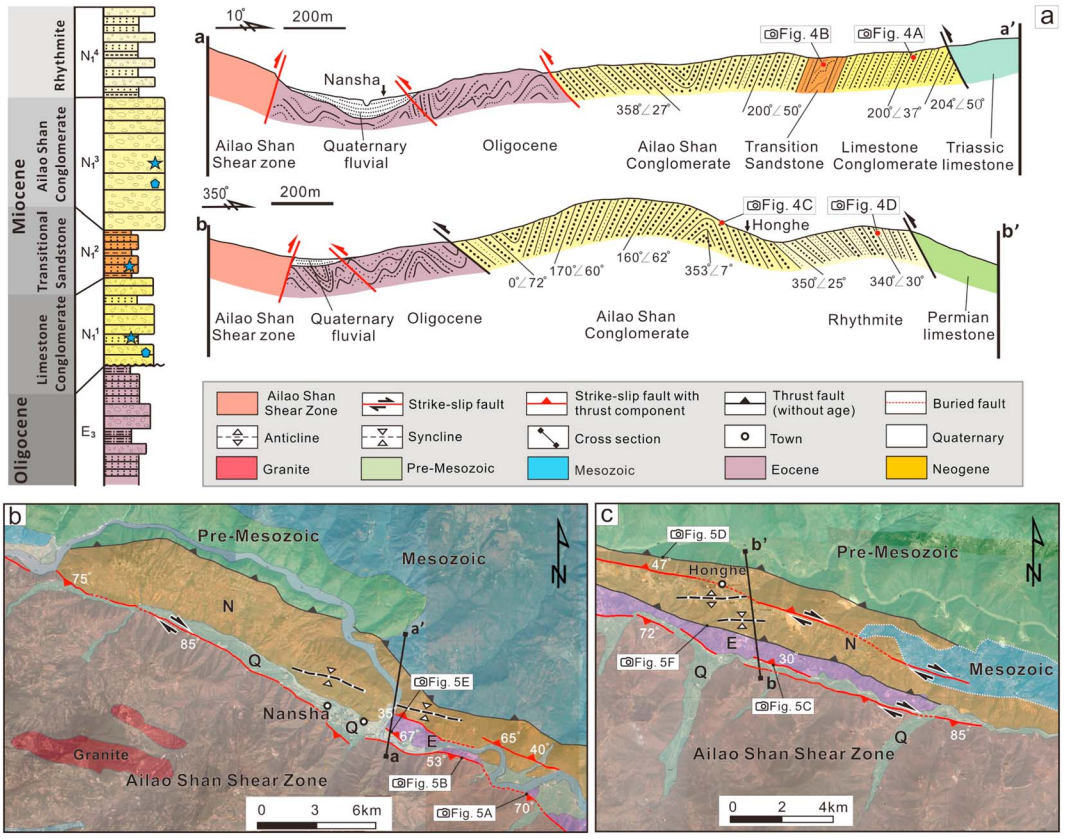

Figure 3. (a) Stratigraphic column and cross sections of the Oligocene-Miocene basin in the major bend area. The Miocene strata consist of four distinct, conformable units, which have been deformed by folding and faulting. They rest unconformably on the Oligocene strata. Blue pentagons are the locations of apatite fission-track samples from *Xiang et al.* [2006, 2007]; blue stars represent fossil locations [*Schoenbohm et al.*, 2005]. (b and c) Geologic maps around the cross sections with the base of Google Earth images. The locations are shown in Figure 2b. Structures and stratigraphic units are based on our field observations and the Geologic Map of Red River Active Fault, scale 1:50,000 [*Guo et al.*, 2013]. Active faults are indicated in red.

The Transitional Sandstone was first reported to overlie the Limestone Conglomerate by *Schoenbohm et al.* [2005]. We found that this unit is just tens of meters thick in the Nansha area (transect a-a′, Figures 3a and 3b) and contains fine-grained sandstone with interbedded mudstone (Figure 4b). This unit is in conformable depositional contact with the overlying and underlying sediments. Biostratigraphy yields Miocene ages for this unit [*Schoenbohm et al.*, 2005].

In contrast to the underlying units, the overlying Ailao Shan Conglomerate is dominated by clasts derived from the Ailao Shan Shear Zone. Our observations indicate that the mylonite clasts, which are often tens of centimeters in diameter, are well rounded in the Honghe area (transect b-b′, Figures 3a, 3c, and 4c). Here the unit is less than 1000 m thick and is thrust over the Oligocene strata. In the Nansha area (transect a-a′), we observe that this unit contains poorly sorted and pebble-sized clasts with sandy interbeds. Fossils previously collected in the Ailao Shan Conglomerate are Miocene in age [*Schoenbohm et al.*, 2005]. The depositional age is constrained by an AFT date of 11.4 ± 0.7 Ma from this unit (Figure 3a) [*Xiang et al.*, 2007].

We describe a new unit called the Rhythmite, which overlies the Ailao Shan Conglomerate (Figure 3a). It is characterized by rhythmic, gray, and yellow sandstone and conglomerate with interbeded mudstone. The conglomerate clasts are composed of pebble-sized gneisses, sandstone, and limestone (Figure 4d). We infer this unit to be Miocene in age because of a lack of apparent structural discontinuity between the Rhythmite and the Ailao Shan Conglomerate.

Since the Miocene sedimentary strata are only found in the narrow Red River valley, it can be inferred that they are dominantly fluvial in origin. Poorly sorted and coarser-grained strata within the section are attributed to input from tributaries that drained the Ailao Shan range [*Schoenbohm et al.*, 2005].

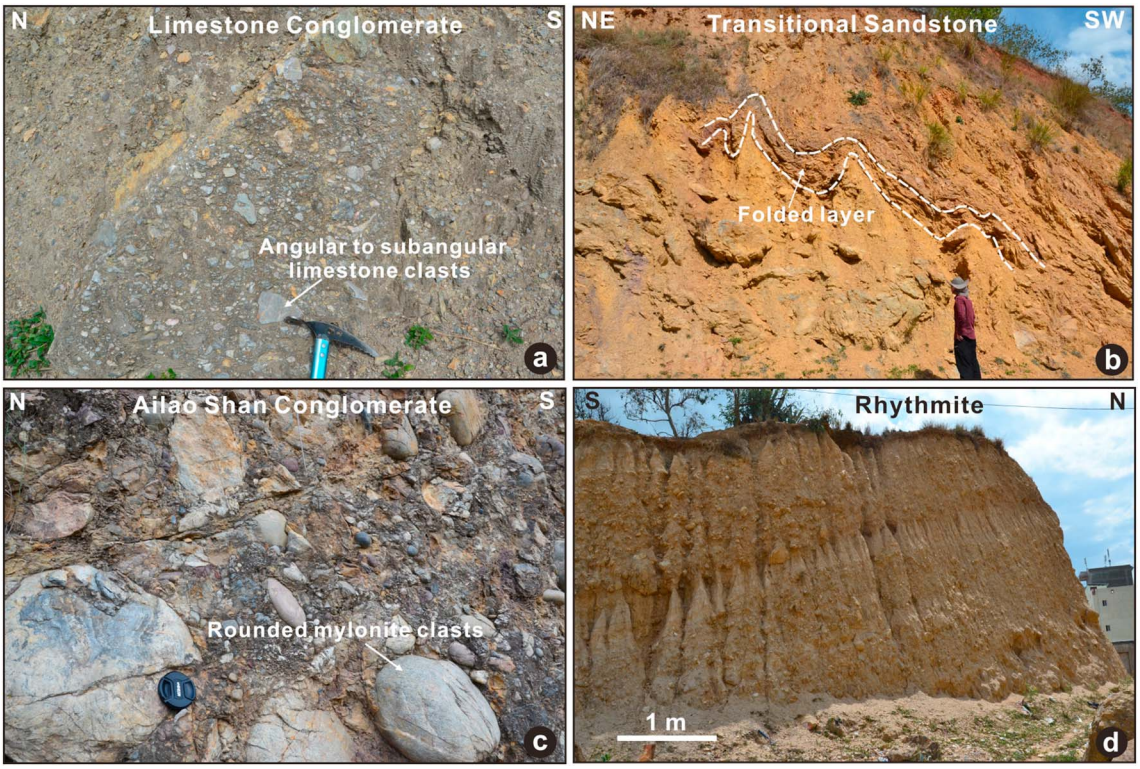

Figure 4. Photos of the Miocene strata. (a) The Limestone Conglomerate characterized by poorly sorted, angular to subangular clasts in a fine matrix. (b) The Transitional Sandstone containing fine-grained sandstone with interbeded mudstone, which is intensely folded. (c) The Ailao Shan Conglomerate containing well-rounded and cobble-sized mylonite clasts. (d) The Rhythmite characterized by rhythmic sandstone and conglomerate.

3.2. Structure

Deformation in the bend area is complex, with features associated with exhumation of the shear zone largely overprinted by later deformation associated with movement along the Red River fault. Shortening structures are extensive, consisting of folds and faults, most with an apparent thrust component.

3.2.1. Folds

The Oligocene and Miocene strata are overthrust by bedrock on both sides, which lead to folding strata and topography buildup. In the Nansha area (transect a-a′, Figure 3a), the Miocene strata form a broad syncline, with limbs dipping at 27–50°. The axial plane strikes WNW, indicating NNE shortening (Figure 3b). Sequential Miocene deposits are observed on the northern limb with a thickness of more than 800 m. Additional asymmetric folds are developed within the Transitional Sandstone (Figure 4b). The Rhythmite does not outcrop in this section possibly due to erosional removal. In the Honghe area (transect b-b′, Figure 3a), the Miocene strata more than 1000 m thick have been deformed into an anticline-syncline pair. The axial planes strike nearly E-W, trending slightly oblique to the Red River valley, indicating N-S shortening (Figure 3c). The Rhythmite inclines north on the northern limb, but this unit does not outcrop on the southern limb of the fold maybe due to erosional removal; the Ailao Shan Conglomerate therefore forms the core of these folds (transect b-b′, Figure 3a). Although sedimentary bedding is cryptic, the orientation of conglomerate layers can be identified by measuring the axial plane of imbricated clasts. In the hinges, the strata are horizontal. On the limbs, clasts dip at 35–72° (transect b-b′, Figure 3a). The Limestone Conglomerate and Transitional Sandstone are not exposed along transect b-b′. The degree of deformation implies significant motion on the basin-bounding thrust faults as well as the Mid Valley fault, but because of a lack of cutoff points across the major faults, the poor exposure, partial erosional removal, and the complexity of deformation, it is not possible to estimate the amount of shortening. Further, thrust and strike-slip displacement has obscured the original contact between the Miocene and Oligocene units.

3.2.2. Faults

The Red River fault consists of two parallel strands in the major bend area: the Range Front fault and the Mid Valley fault (Figure 2b) [*Allen et al.*, 1984]. The Range Front fault follows the base of the Ailao Shan range. It

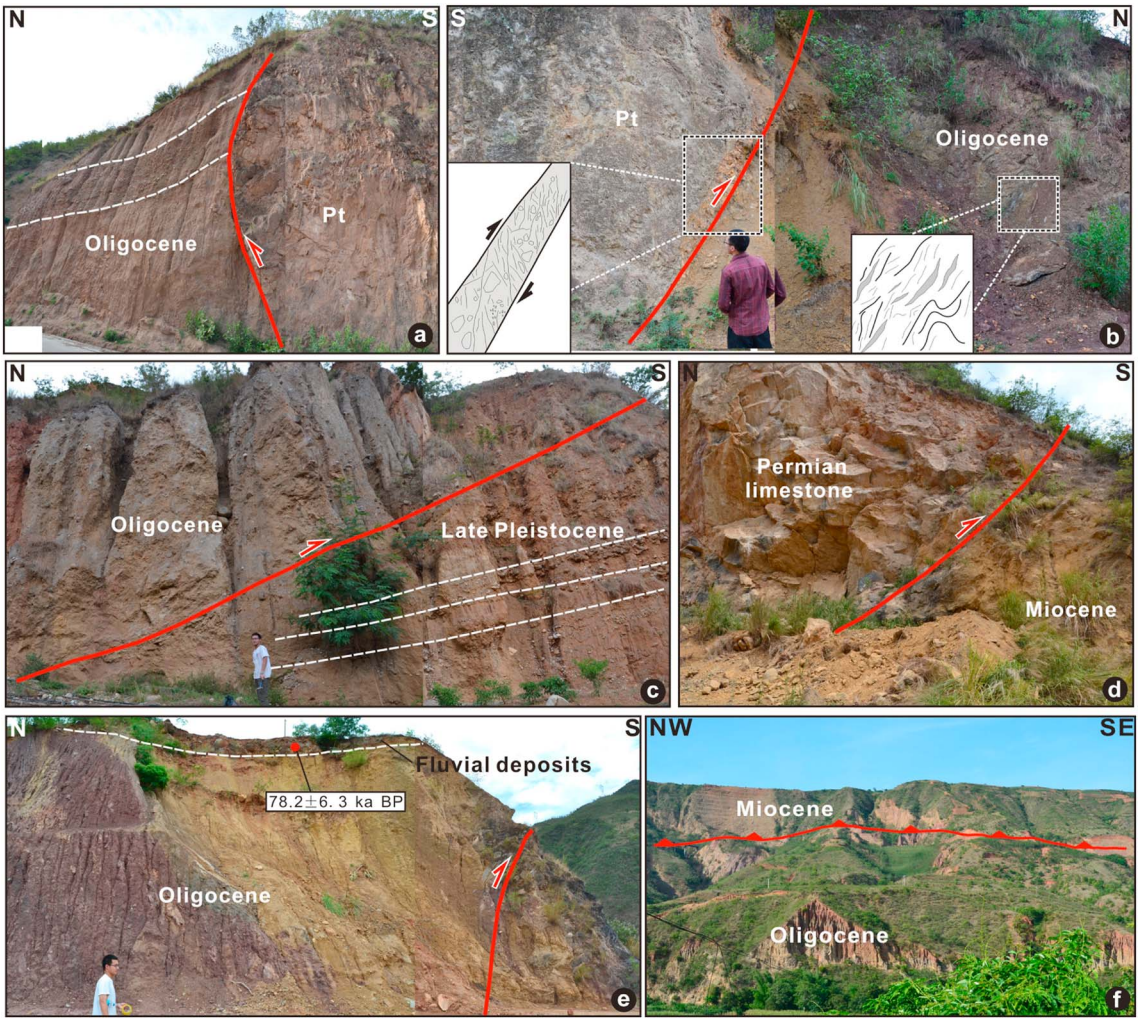

Figure 5. Photos of shortening structures. (a and b) Gneisses of the Ailao Shan Shear Zone are thrust over the Oligocene strata along the Range Front fault. (c) Oligocene sandstone is thrust over late Pleistocene proluvial deposits along the Mid Valley fault. (d) Bedrock is thrust over the Miocene strata along the northern basin margin. (e) Late Pleistocene fluvial gravels with a thermoluminescence date of 78.2 ± 6.3 ka B.P. [*Guo et al*., 2013] are deposited on the hanging wall of the Mid Valley fault, 40 m above the modern Red River. (f) The Miocene strata are thrust over the Oligocene in the Honghe area.

strikes N60°–70°W and dips toward the shear zone at 50–85° (Figures 3b and 3c), marking the southwestern boundary of the Oligocene-Miocene basin. Most observed exposures of the Range Front fault reveal an apparent thrust component, placing Ailao Shan metamorphic rocks over the Oligocene and Miocene strata. For example, in the southeast of Nansha (Figure 3b), our observations indicate that the gneisses are thrust over the Oligocene sandstone along a fault striking N62°W and dipping toward the SW at 70° (Figure 5a). Subhorizontal Oligocene strata in the footwall have been dragged up, suggesting reverse displacement (Figure 5a). The bedrock of the shear zone adjacent to the fault plane is highly fractured. The clast aggregates, as well as laminated lenticles and crumpled textures in the underlying Oligocene strata, indicate a thrust sense of displacement (Figure 5b). Triangular facets developed along the Range Front fault, which according to our observations dip toward the NNE at 30°–50° with heights of 80–180 m, have been interpreted to reflect a normal component of motion along the fault [*Tapponnier et al*., 1990; *Replumaz et al*., 2001]. However, such facets may instead result from differential erosion along the foliation of the Ailao Shan Shear Zone, which is subvertical but often dips slightly valleyward [*Allen et al*., 1984]. Although we do not observe Quaternary sediments affected by the Range Front fault likely due to a lack of deposition, poor exposures, or fault quiescence, *Guo et al*. [2013] reported that the fault cuts through Pleistocene sandy mud in the Yuanjiang area.

The Mid Valley fault is located 1 to 3 km northeast of the Range Front fault (Figure 2b) [*Allen et al*., 1984; *Replumaz et al*., 2001; *Schoenbohm et al*., 2006a; *Guo et al*., 2013]. According to our observations, it is geometrically complex, with discontinuous, stepping, and parallel stands along its trace (Figures 3b and 3c). It cuts through the Oligocene-Miocene strata and Quaternary deposits. The fault dips toward the NNE at 30°–70°, and it reveals right-lateral strike slip with a thrust component. Geomorphic features such as shutter ridges and offset tributaries are well developed along its trace, showing evidence of active right-lateral faulting in the Quaternary. Between the towns of Honghe and Nansha, most of the large tributaries of the Red River show right-lateral offsets between 3 and 10 km where they flow across the Mid Valley fault [*Replumaz et al*., 2001]. A thrust component is also recorded along the Mid Valley fault in the major bend area. Southeast of Honghe (Figure 3c), Oligocene sandstone is thrust over late Pleistocene proluvial deposits along a N20°E dipping fault. The fault is marked by a few centimeters thick, intensely sheared fault gouge, and footwall gravel beds have been deflected downward within 20 m of the fault plane as a result of overthrusting (Figure 5c). East of Nansha (Figure 3b), a thrust fault which dips toward the NNE at 67° developed in the intensely deformed Oligocene strata (Figure 5e). The late Pleistocene fluvial gravels with a thermoluminescence date of 78.2 ± 6.3 ka B.P. [*Guo et al*., 2013] are deposited on the hanging wall, 40 m above the modern Red River.

"Older" faults, which may be inactive today, can also be observed in the Oligocene-Miocene basin. Bedrock is thrust over the Miocene strata on the northern basin boundary (Figure 5d). The thrust fault between the Miocene and Oligocene strata is well exposed in the Honghe area, placing the Ailao Shan Conglomerate over the Oligocene (Figure 5f).

4. Apatite (U-Th)/He Thermochronology

Low-temperature thermochronology records exhumation of the shallow crust, from 2 to 4 km depth. We utilize the elevation dependency of apatite (U-Th)/He (AHe) with closure temperatures of 60–80°C [*Farley*, 2000; *Flowers et al*., 2009] and thermal modeling to determine unroofing history of the Ailao Shan Shear Zone during the middle–late Miocene.

4.1. Sample Descriptions and Results

Nine samples were collected for AHe thermochronologic analysis from granitoids, amphibolites, and granite gneisses in the Ailao Shan Shear Zone (Figure 2b). There are no large-scale granite intrusions along the sample transects, although some granitoids and diorite dikes are present and may result from shear heating during left-lateral displacement [*Leloup et al*., 1995, 2001]. We collected five samples along the Nansha transect which extends over a horizontal distance of 11 km spanning 1116 m in elevation (from 391 to 1507 m, samples 20–30; Figures 2b and 6a). Four samples were collected along the Yuanjiang transect which spans 876 m of vertical relief (from 434 to 1310 m) over a horizontal distance of 13 km (sample 01–13; Figures 2b and 6c). Analytical work was conducted in $^{40}Ar/^{39}Ar$ and (U-Th)/He geochronology laboratory of the Institute of Geology and Geophysics, Chinese Academy of Sciences. Methods are described in the supporting information [*McDowell et al*., 2005] and *Wu et al*. [2016]. Three to five apatite grains were analyzed for each sample. A summary of all individual and mean AHe analyses is presented in Table 1. Errors on the grain AHe dates (1σ) are based on analytical uncertainty in U, Th, and He measurements. For each sample with multiple replicates, a mean and standard deviation are calculated for the spread of replicate analyses (Table 1). We identified one AHe grain date as an outlier (10-G3), as it is different by approximately two standard errors from the rest of replicates for sample 10. This grain is characterized by high effective uranium (eU, Table 1), while the other two grains exhibit similar values. In addition, there is no good fit in the inverse model for sample 10 with this grain. For all of these reasons, we exclude it from the mean calculation.

Samples of the Nansha transect yield AHe dates ranging from 10.9 ± 0.9 to 15.9 ± 1.0 Ma (Figure 6a and Table 1), showing positive date-elevation gradients (Figure 6b). The date-elevation plot defines a gentle gradient from ca. 16 to 13 Ma; although this phase is only defined by the upper two samples, the uppermost sample (30) is significantly older than all the lower elevation samples. A steeper trend in the date-elevation plot begins at ca. 13 Ma, lasting 2–3 Myr, which possibly indicate an accelerated cooling event. AHe dates in the Yuanjiang transect range from 17.0 ± 3.1 Ma at 1310 m to 7.0 ± 1.5 Ma at the base of the transect (434 m) (Figure 6c and Table 1). AHe dates of the four samples correlate positively with elevation. The date-elevation relationship shows a similar pattern to the Nansha transect, with a gentle gradient from ca. 17 to 13 Ma, followed by a steeper, although less well defined, trend (Figure 6d).

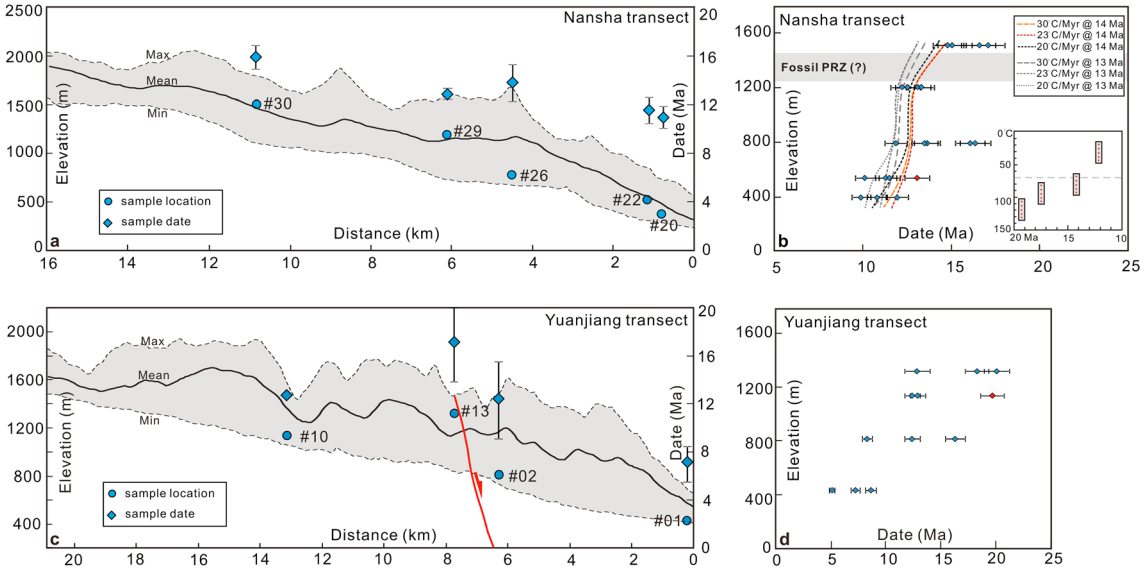

Figure 6. (a and b) Apatite (U-Th)/He thermochronology results from the Nansha transect. (c and d) Apatite (U-Th)/He thermochronology results from the Yuanjiang transect. Grains with high eU are indicated in red. Error bar represents standard deviation for multigrain replicate dates of each sample and 1σ analytical uncertainty in U, Th, and He measurements. Forward modeling was conducted using the thermal history inferred from the date-elevation profile (showing in the inset); see text for details. Dashed lines show preferred model results. Timing and cooling rate of fast cooling are indicated.

4.2. Thermal Modeling

We first utilized the HeFTy program (v.1.8.3.68) [*Ketcham*, 2005] for inverse modeling for single-sample data. Then, the thermal history of AHe date-elevation transect was simulated with the QTQt program (v 5.4.0) [*Gallagher*, 2012] in order to model samples jointly. Finally, we created a sample column for forward modeling using the thermal history inferred from the date-elevation profiles and explore its thermochronologic dates with the observed dates. When combined, the date-elevation relationship and inverse and forward model results allow us to better constrain the thermal history of the shear zone and justify our treatment of our sample transect as vertical profile.

4.2.1. Inverse Model

Individual samples were modeled using the HeFTy program [*Ketcham*, 2005] with the diffusion properties of *Flowers et al*. [2009]. We modeled multiple rather than single grains per sample, which may significantly restrict the spectrum of viable paths [*Ault et al*., 2009]. Additional constraints taken into account in the thermal modeling were as follows: (i) present-day mean surface temperature of 20°C and (ii) an initial time-temperature constraint set at 100–120°C from 27–16 Ma (for older samples) and 20–15 Ma (for younger samples) in order to leave much of the *t-T* space for the early history broadly filled with possible solutions. Sample 30 is the highest sample of the Nansha transect, collected approximately 230 m below the low-relief geomorphic surface. Model results suggest cooling prior to 16 Ma (Figure 7a). The four lower samples (20, 22, 26, and 29) from the same transect reveal similar thermal histories and collectively indicate a later cooling interval that began at 14–13 Ma and lasted 2–3 Myr (Figures 7b and 7c), which is consistent with the thermal history indicated by the date-elevation relationship (Figure 6b) (we show only results for samples 29 and 20 because of the similarity of results for all the four samples). The samples underwent approximately 60°C of cooling to the near Earth's surface during this interval. This translates to an exhumation rate of approximately 0.7–1.0 km/Myr based on a geothermal gradient of 30°C/km. Model results for the Yuanjiang transect (Figures 7d and 7e) suggest a similar thermal history to the Nansha transect. The inverse model result for the highest sample, which was collected approximately 400 m below the low-relief geomorphic surface, suggests an earlier cooling event before 18 Ma (Figure 7d). Model results for the lower samples (02 and 10) indicate approximately 70°C of fast cooling to the near Earth's surface during 2–3 Myr (Figure 7e), which equates to an exhumation rate of approximately 0.7–1.2 km/Myr based on a geothermal gradient of 30°C/km.

All data from the Nansha transect were then modeled with the QTQt program [*Gallagher*, 2012], assuming a consistent vertical separation, same as the present elevation difference between samples. The initial temperature constraint is set 100 ± 20°C at 18 ± 5 Ma and a 35 ± 35°C temperature offset between the uppermost and

AGU Tectonics

10.1002/2016TC004229

Table 1. Results for Apatite (U-Th)/He Thermochronology

Sample ID	U (ppm)	Th (ppm)	He (nmol/g)	eU[a] (ppm)	Mass (μg)	Radius (μm)	Length (μm)	F_T[b]	Date (Ma)	±σ[c] (Ma)	Cor Date (Ma)	± σ (Ma)	Mean Date (Ma)	± σ[d] (Ma)	Latitude	Longtitude	Elevation (m)	Rock Type
20-G1	7.2	2.6	8.9	7.8	4.7	99.0	482.0	0.87	9.4	0.2	10.8	0.6	10.9	0.9	23°13′16″	102°49′2″	391.0	Granitoid
20-G2	10.4	1.9	10.6	10.9	1.4	66.5	318.0	0.81	8.0	0.2	9.9	0.5						
20-G4	8.0	1.7	10.1	8.4	2.4	87.5	316.0	0.84	10.0	0.2	11.9	0.6						
22-G1	36.5	7.6	37.2	38.3	0.9	68.0	189.0	0.80	8.1	0.2	10.1	0.6	11.5	1.1	23°12′46″	102°49′28″	535.0	Amphibolite
22-G2	114.7	22.2	154.7	119.9	1.4	71.8	264.0	0.82	10.7	0.2	13.1	0.7						
22-G3	34.1	7.1	41.9	35.7	2.6	104.3	241.0	0.86	9.7	0.2	11.3	0.6						
22-G4	26.7	2.8	33.5	27.4	3.5	104.8	321.0	0.88	10.1	0.2	11.5	0.6						
26-G1	16.7	36.2	41.1	25.2	1.6	76.5	280.0	0.84	13.4	0.3	16.0	0.9	13.8	1.5	23°11′0″	102°48′53″	790.0	Granite gneisses
26-G3	10.4	20.7	21.2	15.2	2.2	91.0	268.0	0.84	11.5	0.2	13.6	0.7						
26-G4	15.0	32.1	29.2	22.6	1.0	64.8	241.0	0.79	10.7	0.2	13.5	0.7						
26-G6	13.3	29.1	33.4	20.1	2.2	87.0	285.0	0.84	13.7	0.2	16.3	0.9						
26-G7	12.3	27.7	22.6	18.8	2.0	89.0	247.0	0.84	9.9	0.2	11.9	0.6						
29-G2	20.6	30.7	37.8	27.8	3.1	100.0	308.0	0.86	11.2	0.2	13.1	0.7	12.8	0.5	23°11′6″	102°47′15″	1200.0	Granitoid
29-G4	19.2	32.0	32.2	26.8	0.8	54.8	267.0	0.75	9.9	0.2	13.3	0.7						
29-G5	18.8	30.2	31.1	25.9	1.4	71.5	275.0	0.81	9.9	0.2	12.2	0.7						
29-G6	12.8	19.1	22.3	17.3	2.5	101.5	246.0	0.85	10.7	0.2	12.5	0.7						
30-G1	7.3	2.8	13.9	8.0	2.2	88.5	275.0	0.85	14.4	0.3	17.1	0.9	15.9	1.0	23°09′18″	102°44′59″	1507.0	Amphibolite
30-G2	19.9	6.1	31.5	21.4	1.2	71.0	230.0	0.81	12.2	0.2	15.0	0.8						
30-G3	12.5	5.4	22.7	13.8	1.5	76.0	258.0	0.82	13.7	0.3	16.6	0.9						
30-G4	12.9	4.5	20.7	14.0	1.7	78.0	284.0	0.83	12.3	0.3	14.8	0.8						
01-G1	40.1	25.9	38.1	46.2	1.0	59.5	282.0	0.79	6.8	0.1	8.7	0.5	7.0	1.5	23°35′14″	101°57′50″	434.0	Granite gneisses
01-G2	18.1	20.8	15.7	23.0	0.8	58.5	241.0	0.78	5.6	0.1	7.3	0.4						
01-G4	31.2	9.6	15.6	33.4	0.6	51.0	221.0	0.75	3.9	0.1	5.1	0.3						
02-G1	26.5	32.6	49.5	34.1	0.4	50.5	170.0	0.74	12.0	0.2	16.3	0.9	12.3	3.3	23°32′43″	101°55′0″	810.0	Granite gneisses
02-G2	21.7	25.5	20.5	27.7	0.6	47.0	260.0	0.74	6.1	0.1	8.3	0.5						
02-G3	34.9	28.8	48.0	41.7	0.7	55.5	240.0	0.77	9.5	0.2	12.4	0.7						
10-G1	27.9	6.3	37.5	29.3	2.6	96.0	281.0	0.86	10.6	0.2	12.4	0.7	12.6	0.3	23°30′11″	101°53′26″	1130.0	Granitoid
10-G3	59.9	35.9	121.9	68.4	0.4	53.5	168.0	0.75	14.8	0.3	19.6	1.1						
10-G4	22.9	24.4	34.0	28.7	0.6	58.0	169.0	0.76	9.8	0.2	12.9	0.7						
13-G1	1.2	3.7	2.2	2.1	0.3	43.0	145.0	0.68	8.8	0.7	12.8	1.2	17.0	3.1	23°29′30″	102°00′02″	1310.0	Granite gneisses
13-G2	3.6	1.6	7.5	4.0	0.6	55.0	208.0	0.77	15.3	0.4	20.0	1.1						
13-G4	4.8	2.2	2.2	5.3	0.3	44.5	185.0	0.71	13.0	0.4	18.2	1.1						

[a]eU: effective uranium concentration, a parameter that weights the decay of the two parents for their alpha productivity, by [U] + 0.235*[Th] [*Flowers et al*., 2009].
[b]F_T is the alpha-ejection correction after *Farley et al*. [1996].
[c]Errors on the (U-Th)/He dates (1σ) are based on analytical uncertainty in U, Th, and He measurements.
[d]Standard deviation for the replicate analyses.

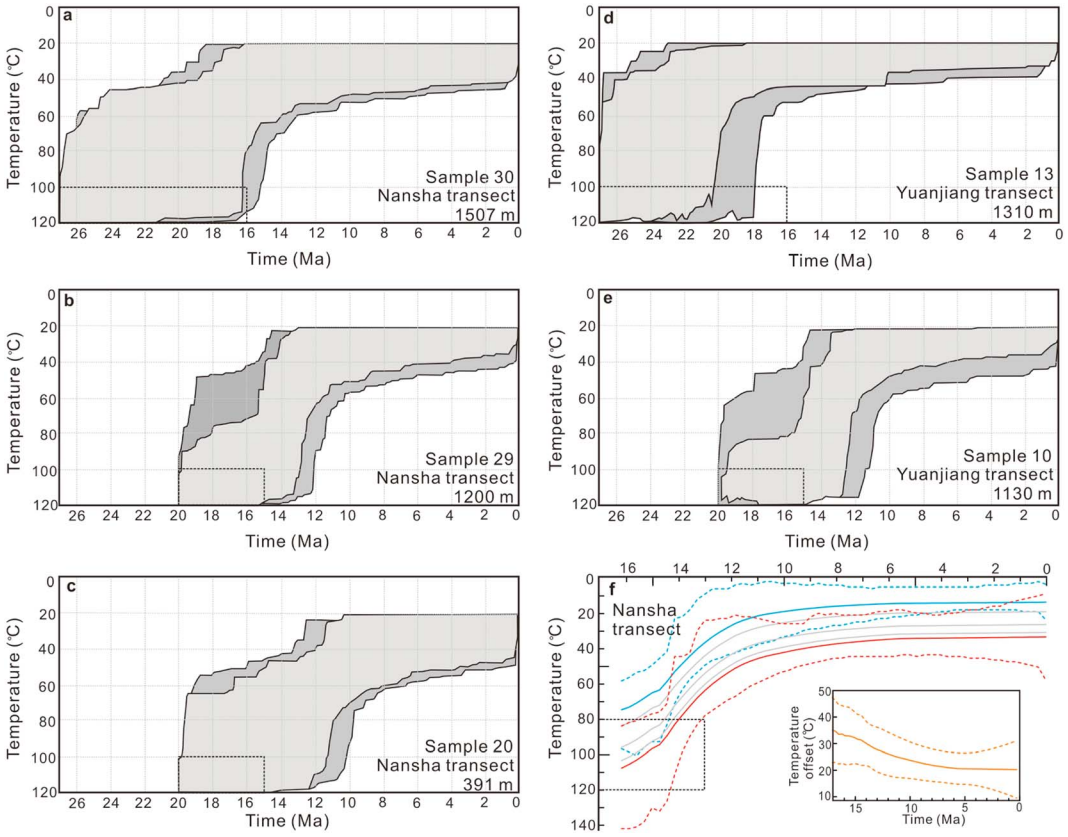

Figure 7. Inverse thermal modeling results. (a–c) Time-temperature models for sample 30, 29, and 20 in the Nansha transect using HeFTy [*Ketcham*, 2005]. (d and e) Time-temperature models for sample 13 and 10 in the Yuanjiang transect using HeFTy [*Ketcham*, 2005]. Swaths represent randomly generated cooling paths that fit the data to an acceptable (dark gray) and good (light gray) standard. The black dotted boxes are initial constraints. (f) Time-temperature history of the Nansha sample transect derived from QTQt modeling [*Gallagher*, 2012]. Blue line corresponds to the uppermost sample (30). Blue dashed lines correspond to 95% confidence interval for this sample. Red line corresponds to the lowermost sample (20). Red dashed lines represent 95% confidence interval for this sample. Gray lines represent the three middle samples. The inset shows the history of temperature offset between the uppermost and lowermost samples indicated by the orange line. Orange dashed lines represent 95% confidence interval.

lowermost samples. The model results suggest a phase of cooling at ca. 15 Ma (Figure 7f), consistent with thermal histories revealed by the HeFTy models and the date-elevation plot. The temperature offset between the uppermost and lowermost samples suggests a value of 35–32°C until 15 Ma, followed by a decrease to 20°C from 15 to 10 Ma (inset of Figure 7f).

4.2.2. Forward Model

In order to further justify the thermal history inferred from our date-elevation profiles and whether the sample transect can be treated as vertical profile, a suite of individual forward models was conducted to estimate the cooling history of the Nansha transect, according to the following scenario. We assume that the samples of the Nansha transect are from a vertical column with constant spatial separation between them. We suppose that an earlier cooling event brought sample 30 to reside near the base of partial retention zone (PRZ) for helium diffusion. After a period of slow cooling or isothermal holding, the second fast cooling event brought the lower four samples through the PRZ (inset of Figure 6b). We derive monotonic *t-T* histories, using a range of parameters, including the onset of rapid cooling (12, 13, or 14 Ma), cooling rates (20, 23, or 30°C/Myr), and magnitude of cooling (50, 60, or 70°C). Predicted dates were calculated using the HeFTy program by prescribing identical thermal histories with respect to the onset and cooling rate [*Lease et al.*, 2011]. The RDAAM model was used with the typical concentrations of U, Th, and grain dimensions [*Flowers et al.*, 2009]. Our preferred models are shown in Figure 6b, which are consistent with the date-elevation data and inverse model results. We do not conduct forward modeling of the Yuanjiang transect because vertical displacement might have occurred within the transect.

5. Discussion

5.1. Origin and Significance of the Major Bend

The major bend is a prominent feature of the Ailao Shan-Red River fault. The geometry of the bend, a change from the overall trend of N40°–50°W to N60°–70°W in the bend area (Figure 2a), would result in a releasing bend during the early left-lateral phase of movement and a restraining bend during right-lateral reactivation along the Red River fault. Our data support this hypothesis. Releasing bends are characterized by significant basin sedimentation and oblique deformation [*Cunningham and Mann*, 2007]. The Miocene strata in the bend area are approximately 2000 m thick and are notably absent north the bend. They are generally poorly sorted, coarser-grained fluvial sediments, input from tributaries along the valley and deposited in the depressed area along the bend. It is possible that the sediments originally covered a larger region but have only been preserved in the bend region. However, given their thickness (approximately 2000 m) and unique association with the major bend, a releasing basin setting is more likely. Unfortunately, we do not observe structural evidence for an earlier phase of normal displacement relating to the Miocene deposition in the bend area likely because they were overprinted by widespread transpressional tectonism after right-lateral reactivation along the Red River fault. An important consideration for understanding the evolution of fault bends is whether or not they migrate along strike with increased displacement. We argue that the location of the major bend remains relatively fixed with respect to adjacent laterally moving blocks for several reasons. First, the onset of left-lateral shearing is estimated to be ca. 34 Ma, but deposition of the lowest unit of the Miocene, as revealed by AFT dates, started after 20 Ma. Therefore, the displacement after the bend formation should be much less than the total left-lateral displacement. Second, fixed releasing bends tend to host sediments with significant thickness [*Cunningham and Mann*, 2007], which is consistent with a documented approximately 2000 m thickness for the Miocene strata in our study area. Third, we also argue for little translation during the later right-lateral phase of movement as the Miocene strata are distributed northeast of the Range Front fault, which will not cause displacement, and the Mid Valley fault which does cut through the Miocene has experienced a maximum displacement of 22 km in the bend area [*Replumaz et al*., 2001]. Given approximately 130 km length of the basin, the effect of such displacement is minor.

We find evidence for the restraining bend during the right-lateral phase of deformation as well. Restraining bends are sites of oblique-slip displacement and topographic uplift [*Cunningham and Mann*, 2007]. In the major bend, our observations indicate both the Range Front fault and Mid Valley fault experienced transpressional right-lateral strike-slip movement. However, an apparent normal component along the Range Front fault has been documented northwest of the bend, resulting in triangular facets, Quaternary sedimentary basins, and partial exhumation of the Ailao Shan gneisses [*Tapponnier et al*., 1990; *Leloup et al*., 1995; *Replumaz et al*., 2001]. Miocene strata in the bend are now deformed by nearly E-W oriented folds, forming relatively high topography (approximately 300–500 m higher than the modern river) in the Red River valley, as a result of shortening. We also observe thrusting of bedrock on both margins over the basin. These observations suggest formation of a restraining bend even though the Red River valley may be overall dominated by transtension (Figure 2a).

If our hypothesis is correct, the major bend must have formed during the left-lateral phase of deformation along the Ailao Shan-Red River fault, earlier than previously thought. *E. Wang et al*. [1998] argued that the bend was caused by displacement along the Xianshuihe-Xiaojiang fault system; as the Sichuan-Yunnan block was translated along the left-lateral fault system, it impinged on and deformed the Ailao Shan-Red River fault. However, our data suggest that the major bend formed much earlier than initiation of the Xianshuihe-Xiaojiang fault system, as it was responsible for formation of the Oligocene-Miocene basin in the bend region. The basin formation can be constrained by the depositional age of the Limestone Conglomerate (20.7 ± 2.4 Ma and 20.8 ± 7.8 Ma revealed by AFT dates). Additional displacement along the Xianshuihe-Xiaojiang fault system could have further deflected the bend area after its formation. There could be a genetic relationship between the bend and the Xiaojiang fault; the bend may have localized near a preexisting structure that then later controlled the location of the Xiaojiang fault. The Qujiang and Jianshui faults lie to the north of and subparallel to the bend area in the southeastern tip of the Sichuan-Yunnan block (Figure 1b). They show an apparent thrust component, inferred to absorb a part of left-lateral motion of the Xiaojiang fault [*Wang et al*., 2014]. Those observations suggest the SE movement of the Sichuan-Yunnan block causes transpression in the southeastern tip of the block as well as some bending of the Ailao Shan-Red River fault.

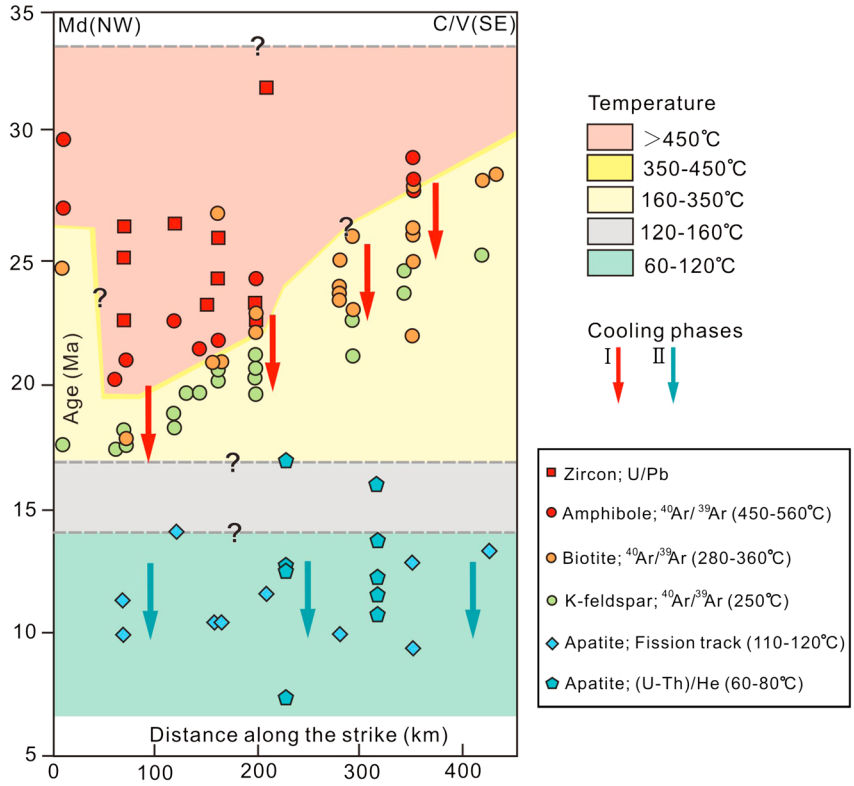

Figure 8. Summary of thermochronologic data for the Ailao Shan Shear Zone from Midu (Md) in the northwest to the China/Vietnam border (C/V) indicated in Figure 2a (after *Leloup et al.* [2001]). Ages are compiled from *Chen et al.* [1993], *Leloup et al.* [2001], *Harrison et al.* [1996], *Bergman et al.* [1997], *Xiang et al.* [2006, 2007], *Chen et al.* [2015], and this study.

5.2. Thermal History

Our AHe data, when combined with sedimentology, structural geology, geomorphology, and existing thermochronologic data, suggest both an early (ca. 27–17 Ma) and a late (ca. 14–10 Ma) phases of rapid exhumation (Figure 8).

The first rapid exhumation event during left-lateral movement has previously been recognized. $^{40}Ar/^{39}Ar$ dating of amphiboles, biotite, and K-feldspar records cooling through their closure temperatures during exhumation, indicating that the Ailao Shan metamorphic massif was exhumed rapidly to various levels from ca. 27–17 Ma [e.g., *Leloup et al.*, 1995, 2001; *Harrison et al.*, 1996; *P. L. Wang et al.*, 1998]. The existing data show that the rapid cooling began earlier in the southeast and propagated gradually to the northwest through time (Figure 8) [e.g., *Harrison et al.*, 1996; *Leloup et al.*, 2001]. Although we do not see this cooling event clearly in our data, the earlier cooling revealed by samples 13 and 30, the topmost samples in the Yuanjiang and Nansha transects, respectively, may relate to this cooling event.

Our data reveal a second phase of fast cooling beginning at 14–13 Ma and lasting 2–3 Myr. However, since our samples are collected across over a horizontal distance of approximately 10 km, there are two possible interpretations for our AHe data. First, our sample transects can be treated as date-elevation profiles. We feel justified in this treatment, at least for the Nansha transect for the following reasons. First, by the time Ailao Shan gneisses had been exhumed to the near Earth's surface (<3 km), strain was dominated by brittle deformation and displacement was mainly localized on the Range Front fault. There is no evidence for faults with significant vertical displacement within the Ailao Shan range along the Nansha transect, particularly between the uppermost sample 30 and all the lower elevation samples. Second, the single-sample cooling histories revealed by inverse models are quite similar among samples 20, 22, 26, and 29 (Figures 7b and 7c). The uppermost sample (30) reveals a different thermal history probably due to an early cooling event or isothermal holding. Third, forward model under the assumption of a vertical column well fits the date-elevation data. If we are justified in treating our samples as a vertical transect, the steep trend in the date-elevation plot

of the Nansha transect indicates a second accelerated cooling event beginning at ca. 13 Ma, lasting 2–3 Myr, The date-elevation data from the Yuanjiang transect show a similar pattern, with a gentle gradient from ca. 17 to 13 Ma, followed by a steeper, although less well defined, trend (Figure 6d). However, the Yuanjiang transect is complicated by the presence of a fault between sample 02 and 10, the displacement and the timing of which cannot be determined, and cannot therefore be treated as a vertical transect.

A second option is to treat the samples as horizontal transects, given their horizontal separation. Inverse model results from most of the samples show similar cooling pattern: a fast cooling interval during ca. 14–10 Ma. The highest samples (13 and 30), collected below low-relief relict landscape and sample 01, collected near the Range Front fault, show cooling prior to 16 Ma and after 10 Ma, which may be affected by differential erosion and vertical displacement on the Range Front fault, respectively. The faster cooling is restricted to the lower samples, implying relief growth through valley incision with rapid incision superimposed onto a slower background erosional rate, rather than a widespread increase in erosion. In this treatment, we still draw a similar conclusion that a fast cooling occurred before 10 Ma across the Ailao Shan range with formation of incised valley, but we cannot constrain the timing of onset clearly.

Our data suggest a brief, quiescent period between the two phases of cooling from ca. 17 to 13 Ma, probably indicative of slow exhumation through or stasis in the PRZ during this interval (Figure 6b), but we cannot accurately identify the onset and duration of the slow cooling. The period of slow cooling might be short and is less thermochronologically constrained, and therefore, it is possible that exhumation may have occurred uninterrupted from ca. 27 to 10 Ma. However, the sedimentary record, geomorphology, and our thermal modeling also support our argument for two phases of exhumation. First, the Transitional Sandstone and Ailao Shan Conglomerate record an evolution from rounded and fine-grained to poorly sorted and coarser-grained sediments, indicating relief reduction followed by relief production in the middle–late Miocene. Mylonite clasts of the Ailao Shan Conglomerate reach tens of centimeters in diameter; *Xiang et al*. [2007] report an AFT date from a mylonite cobble within this unit of 11.4 ± 0.7 Ma. Further, the longitudinal profiles of tributaries along the Ailao Shan range are segmented, suggesting pulsed uplift after formation of the relict landscape [*Schoenbohm et al*., 2004]. Finally, our forward model for the Nansha transect is well fit the date-elevation data using a two stages cooling history (Figure 6b).

Finally, although we are confident in our interpretation of a two stages exhumation history, we wish to fully rule out any additional complications, such as thermal heterogeneities, differential exhumation caused by fault displacement and river incision, or tectonic diachronism along strike. Stable-isotope evidence and the weakly developed nature of retrograde alteration in the Ailao Shan tend to rule out widespread fluid advection within the massifs [*Leloup and Kienast*, 1993; *Harrison et al*., 1996]. Additionally, after the first fast exhumation, relief reduction along the Ailao Shan range also would have reduced the heterogeneities in the thermal structure. Footwall rotation during vertical displacement on the Range Front fault could result in differential exhumation which would cause across-strike diachronism [*Harrison et al*., 1996]. However, post-Miocene vertical displacement in the major bend area is almost negligible [*Schoenbohm et al*., 2004]. River incision must play an important role in the exhumation of our samples, but would result in elevation-dependent cooling, and would therefore be a minor effect. Along-strike cooling diachronism might have occurred during the second exhumation, which could explain that some AFT dates are younger than our AHe dates (Figure 8), but we cannot identify any along-strike cooling trends due to the limited data set.

5.3. Late Cenozoic Evolution of the Ailao Shan-Red River Fault

When combined with existing studies, our new data from stratigraphy, structural geology, and low-temperature thermochronology enable us to reconstruct the late Cenozoic structural and geomorphic development of the Ailao Shan-Red River fault (Figure 9).

5.3.1. Exhumation of the Ailao Shan Shear Zone, Stage 1

The first stage in the history of the Ailao Shan-Red River region is removal of cover rocks of the shear zone (Figure 9). The exhumation mechanism, whether by transpression [e.g., *E. Wang et al*., 1998] or transtension [e.g., *Harrison et al*., 1996], remains controversial. The spatial and temporal relationship between the Ailao Shan Shear Zone and the Lanping-Simao fold belt in the Indochina block implies regional shortening (Figure 2a) [*E. Wang et al*., 1998; *Schoenbohm et al*., 2005]. Within the shear zone, amphibolite-grade metamorphic rocks are thrust over schist unit (Figure 9); deformation fabrics in the low-grade schist indicate transpression [*Zhang et al*., 2006]. As an alternative, "zipper tectonics" was proposed to explain the diachronism in

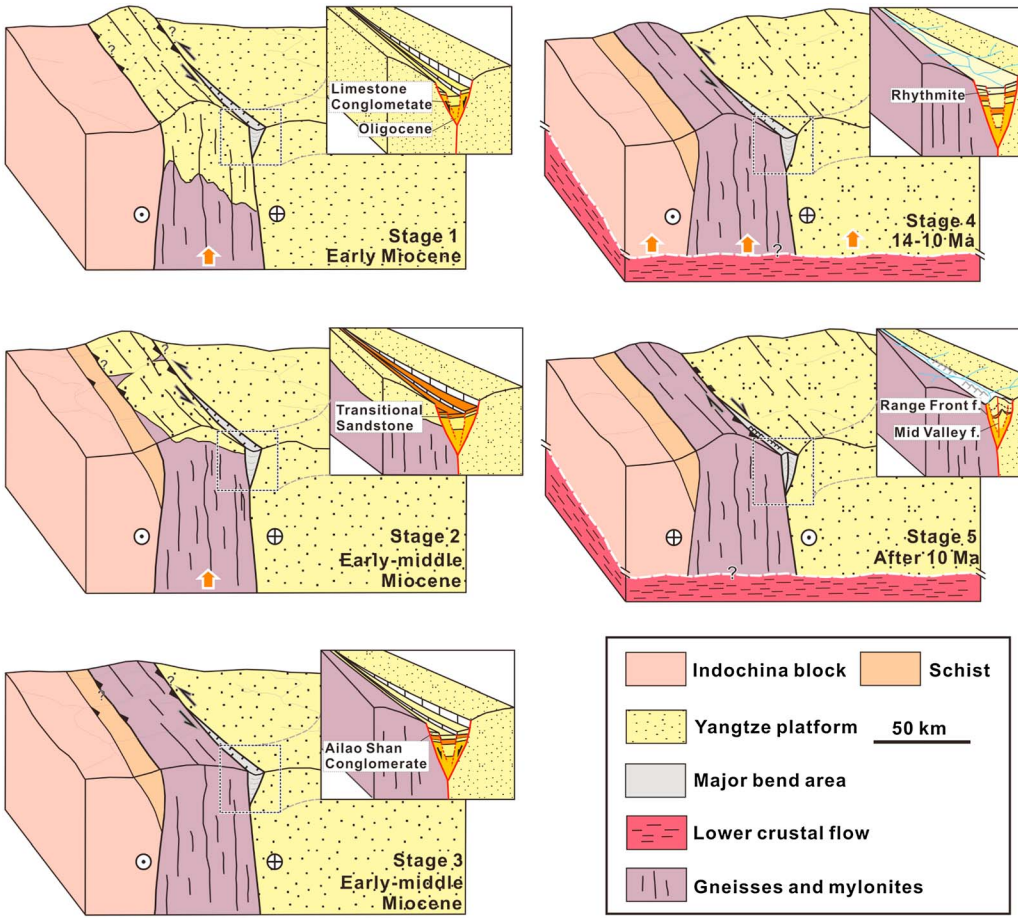

Figure 9. Tectonic and geomorphic evolution along the Ailao Shan-Red River fault. See text for elaboration. The vertical scale is exaggerated approximately 3 times than the horizontal scale. Stage 1 is removal of cover rocks of the shear zone during left-lateral shearing. The inset shows deposition of the Limestone Conglomerate. Stage 2 is continued exhumation of cover and metamorphic rocks but tectonically driven exhumation is ceased. The Transitional Sandstone was deposited in the releasing bend area. In Stage 3 low-relief landscape may have developed along the Ailao Shan range. The sediments from the shear zone gneisses began to be deposit in the Red River valley. In Stage 4 the Ailao Shan range may have risen to its modern elevation with high-relief topography developing due to river incision. The Ailao Shan Conglomerate and the Rhythmite were deposited in the bend area. In Stage 5 reversal of displacement occurred, and the major bend changed to a restraining bend. Deposition ceased, and the Oligocene and Miocene strata were deformed as folds, cut through by faults, and removed by erosion.

cooling along the Ailao Shan range [*Harrison et al.*, 1996; *Leloup et al.*, 2001]. Rocks originally located within the Indochina block along the NW portion of the fault zone first deformed in a transpressional regime, then in pure strike slip near the neutral point (located in Midu, Figure 2a), and finally entered the transtensional domain where extension induced normal faulting, exhumation, and rapid cooling of the shear zone [*Leloup et al.*, 2001]. Since our observations and data are mainly concentrated on the bend area, we cannot determine which model is more accurate. The strike-slip component along the shear zone is the most important: if the left-lateral displacement is 700 ± 200 km [*Leloup et al.*, 1995], a small oblique component, either extensional or contractional, can result in significant exhumation.

Stage 1 unroofing occurred during left-lateral strike slip, marked by deposition of the Limestone Conglomerate at the base of the Miocene strata (Figure 9). These strata are derived exclusively from Yangtze platform rocks, indicating the shear zone gneisses may not expose to the Earth's surface. *Schoenbohm et al.* [2005] suggested that the South China and Indochina blocks were in direct contact prior to exposure of the Ailao Shan metamorphic rocks which were capped by Yangtze platform rocks. These capping rocks were eroded and deposited in the releasing bend region during the early mountain building. By

Stage 2, the Ailao Shan metamorphic rocks had already been exhumed to shallow depths (<2 km) or to the Earth's surface (Figure 9). This phase of rapid exhumation may have occurred from ca. 27 to 17 Ma revealed by $^{40}Ar/^{39}Ar$ dating of amphiboles, biotite, and K-feldspar [e.g., *Leloup et al*., 1995, 2001; *Harrison et al*., 1996].

5.3.2. Postexhumation, Stage 2, and Stage 3

A tectonic quiescence may have occurred in Stage 2 and Stage 3 (Figure 9). Even though tectonically driven exhumation ceased, possibly slow erosion continued as a result of remnant high relief, just not as intensely as before. The capping rocks were totally eroded away, and the Ailao Shan metamorphic rocks were extensively exposed at the Earth's surface. The Transitional Sandstone and the sediments at the base the Ailao Shan Conglomerate may be deposited in this period. During this tectonic quiescence, a low-relief geomorphic surface may have developed in the Ailao Shan range as a result of widespread erosion. The Limestone Conglomerate and Transitional Sandstone record an evolution from subangular and coarser-grained to rounded and fine-grained sediments (Figure 3a). This is typical of the continental molasse, indicating geomorphic evolution from relief development in Stage 1 to removal in Stage 3 along the Ailao Shan range in the early–middle Miocene. These two stages might be characterized by a period of slow cooling, which is indicated by the gentle gradient in our date-elevation data (Figure 6b).

5.3.3. Accelerated Exhumation and Reversal of Displacement

We argue that the last two stages in the evolution of the Ailao Shan-Red River fault consist of accelerated exhumation of the shear zone in Stage 4 and reversal of displacement in Stage 5 (Figure 9). In Stage 4, the Ailao Shan range may have experienced 1400–1500 m surface uplift based on river longitudinal profile analysis [*Schoenbohm et al*., 2004]. High relief developed along the range as a result of river incision (Figure 9). The cobble-sized Ailao Shan Conglomerate and the Rhythmite were deposited in the bend area. Our AHe data from the southern segments of the Ailao Shan range reveal accelerated exhumation at ca. 14–10 Ma. Based on paleoaltimetric studies, *Li et al*. [2015] argued that the Xiaolongtan basin (approximately 70 km northeast of the Nansha transect) in SE Yunnan may have achieved the present-day elevation during 12.7–10 Ma. The AFT samples collected in the northern segment of the Ailao Shan range yield dates of 13–10 Ma. Long, >14 um track lengths suggest rapid cooling (Figure 8) [*Bergman et al*., 1997]. The uplift in this stage might be regional rather than constrained to the shear zone since no obvious vertical displacement is observed in the region on either side of the fault zone [*Schoenbohm et al*., 2006a].

Reversal of displacement occurred in Stage 5. The major bend changed to a restraining bend after right-lateral reactivation along the Red River fault (Figure 9). Deposition ceased, and the Oligocene and Miocene strata in the bend area began to deform through folding and faulting. Based on the seismic analysis and stratigraphic information from confidential exploration wells in the Gulf of Tonkin (Figure 2a), *Fyhn and Phach* [2015] argue that the strike-slip inversion may commence around 10–8 Ma, which is contrary to previous studies indicating latest Miocene left-lateral motion [*Schoenbohm et al*., 2006b]. Right-lateral shearing therefore appears to lag regional uplift. Our AHe data do not reveal an exhumation rate change related to the onset of right-lateral movement.

5.4. Geodynamic Implications

The Ailao Shan Shear Zone experienced accelerated exhumation at ca. 14–10 Ma. It coincides with a suite of significant phenomena in the Tibetan Plateau and its surroundings in the middle–late Miocene (Figure 1b and Table 2) [*Lease et al*., 2011]: (1) the onset of east-west extension in the plateau interior at ca. 15 Ma [e.g., *Blisniuk et al*., 2001; *Williams et al*., 2001]; (2) the rapid river incision in the southeastern margin of the Tibetan Plateau at ca. 13–10 Ma [e.g., *Clark et al*., 2005; *Ouimet et al*., 2010]; (3) the development of new east vergent thrust faults and accelerated exhumation in the northeastern Tibetan Plateau margin at ca. 17–9 Ma [e.g., *Bovet et al*., 2009; *Zheng et al*., 2010; *Yuan et al*., 2011; *Duvall et al*., 2013]; (4) the rapid exhumation of the Longmen Shan at 15–10 Ma [e.g., *Kirby et al*., 2002; *Godard et al*., 2009; *E. Wang et al*., 2012]; (5) the initiation of major strike-slip faults such as Xianshuihe, Ganzi, Kunlun, Jiali, and Haiyuan faults [e.g., *Roger et al*., 1995; *Lee et al*., 2003; *Wang et al*., 2009]; and (6) 40% slowing of India-Asia convergence rates between 20 and 11 Ma [*Molnar and Stock*, 2009].

A possible relationship among these phenomena is debatable, but this coincidence probably suggests a dynamic change in the course of plateau growth, separating distinctly different deformation styles. Initially, after India-Eurasia collision, large fragments of Eurasian lithosphere were extruded out of central Tibet toward southern China and northern Indochina [e.g., *Tapponnier et al*., 1982; *Akciz et al*., 2008]. Displacement was localized on continental-scale shear zones, such as the Gaoligong and Ailao Shan Shear Zones [e.g., *Wang et al*., 2008;

Table 2. Summary of Timing of Deformation

Location[a]	Structure or Location	Timing[b]	Method	Publication
1	Ailao Shan Shear Zone	13–10 Ma	Apatite fission track thermochronology (AFT)	*Bergman et al.* [1997]
2	Diancang Shan	13–4 Ma	$^{40}Ar/^{39}Ar$ thermochronology	*Cao et al.* [2011]
3	Xianshuihe-Xiaojiang fault	~4 Ma	Tectonosedimentology	*E. Wang et al.* [1998]
4	Ailao Shan Shear Zone	~13–10 Ma	(U-Th)/He thermochronology	This study
5	Diancang Shan	~5 Ma	$^{40}Ar/^{39}Ar$ thermochronology	*Leloup et al.* [2001]
6	Anninghe fault	~17 Ma	AFT thermochronology	*S. Wang et al.* [2012]
7	Yangze River	>10 Ma	AFT and (U-Th)/He thermochronology	*Reid et al.* [2005] and *Ouimet et al.* [2010]
8	Yalong River	<14 Ma	(U-Th)/He thermochronology	*Ouimet et al.* [2010]
9	Daocheng granite	22–15 Ma	AFT and (U-Th)/He thermochronology	*Tian et al.* [2014]
10	Dadu River	13–9 Ma	AFT and apatite (U-Th)/He thermochronology	*Clark et al.* [2005]
11	Longmen Shan	12–9 Ma	$^{40}Ar/^{39}Ar$ and (U-Th)/He thermochronology	*Kirby et al.* [2002]
12	Longmen Shan	15–10 Ma	AFT and (U-Th)/He thermochronology	*E. Wang et al.* [2012]
13	Longmen Shan	<20 Ma	(U-Th)/He thermochronology	*Godard et al.* [2009]
14	Xianshuihe fault	12–10 Ma	Zircon U-Pb thermochronology	*Roger et al.* [1995]
15	Danba dome	6–4 Ma	AFT thermochronology	*Jolivet et al.* [2015]
15	Danba dome	~10 Ma	(U-Th)/He thermochronology	*Ouimet et al.* [2010]
16	Jiali fault	18–12 Ma	$^{40}Ar/^{39}Ar$ thermochronology	*Lee et al.* [2003]
17	Ganzi fault	~13 Ma	AFT thermochronology	*Wang et al.* [2009]
18	Litang fault	7–2 Ma	AFT and (U-Th)/He thermochronology	*Zhang et al.* [2015]
19	East Kunlun fault	8–5 Ma	AFT and (U-Th)/He thermochronology	*Duvall et al.* [2013]
20	East Kunlun fault	20–15 Ma	AFT and (U-Th)/He thermochronology	*Yuan et al.* [2006] and *Duvall et al.* [2013]
21	Central Kunlun fault	12–8 Ma	AFT and (U-Th)/He thermochronology	*Duvall et al.* [2013]
22	North Qilian Shan	16–12 Ma	Sedimentatology	*Bovet et al.* [2009]
23	North Qilian Shan	~10 Ma	(U-Th)/He thermochronology	*Zheng et al.* [2010]
24	North Qilian Shan	17–12 Ma	AFT and (U-Th)/He thermochronology	*Duvall et al.* [2013]
25	Qinghai Nan Shan	11–9 Ma	Magnetostratigraphy	*H. Zhang et al.* [2012]
26	Elashan fault	12–6 Ma	Offset and slip rate	*Yuan et al.* [2011]
27	Riyue Shan	13–7 Ma	Offset and slip rate	*Yuan et al.* [2011]
28	Longmen Shan	<20 Ma	AFT thermochronology	*Xu and Kamp* [2000]
29	Litang	~17 Ma	AFT thermochronology	*Lai et al.* [2007]
30	Chola Shan	~17 Ma	AFT thermochronology	*Lai et al.* [2007]
31	Yumu Shan	9.8–9.6 Ma	Paleomagnetic dating and tectonosedimentology	*Fang et al.* [2013]
32	North Qilian Shan	9–5 Ma	AFT thermochronology	*Jolivet et al.* [2001]

[a]Refer to Figure 1b for locations.
[b]Timing of initiation or accelebrated fault movement or bedrock exhumation.

B. Zhang et al., 2012; *Liu et al.*, 2012]. As plate convergence continued, however, hot and fluid rich low–middle crust developed in the central plateau [*Nelson et al.*, 1996]. Lower crust material flowed outward from the plateau driven by gravity [e.g., *Clark et al.*, 2006; *Royden et al.*, 2008]. This marks a transition from early extrusion of Tibetan lithosphere to flow of a viscous lithosphere. The injection of lower crust would have inflated crustal thickness and caused passive surface uplift [*Royden et al.*, 1997, 2008], which may have triggered the ca. 14–10 Ma accelerated exhumation we observe in the Ailao Shan Shear Zone and its surroundings.

However, the timing of lower crustal flow remains uncertain despite the decades of studies. For example, in the southeastern margin of the Tibetan Plateau, rapid cooling and exhumation related to regional uplift, inferred from thermochronology, show much variation (ca. 20–5 Ma) [e.g., *Kirby et al.*, 2002; *Clark et al.*, 2005; *Ouimet et al.*, 2010; *E. Wang et al.*, 2012; *Tian et al.*, 2014]. Recent paleoaltimetry studies argue that present-day elevations may have been achieved in NW Yunnan since the latest middle Eocene (ca. 40 Ma) [*Hoke et al.*, 2014] and in SE Yunnan since the middle Miocene (12.7–10 Ma) [*Li et al.*, 2015]. However, these thermochronologic and paleoaltimetric data are not mutually exclusive and may reflect several factors. First, crustal thickening may have occurred in SE Tibet and NW Yunnan at early stages of India-Asia continental collision. Second, uneven flow would result in nonuniform surface uplift: magnetotelluric imaging [*Bai et al.*, 2010] suggests that lower crustal material flows in channels rather than sheets. Third, crustal flow is a continuous process through time, and it could induce successive phases of deformation at the Earth's surface. Fourth, climate change and local effects, such as faulting and glaciation, could also cause some of the differences in timing [e.g., *Ouimet et al.*, 2010; *Zhang et al.*, 2015; *Zhang et al.*, 2016]. For example, the late Miocene to present monsoon may have resulted in more precipitation and seasonal variability in the SE Tibetan Plateau, leading to enhanced late

Miocene to present river incision (ca. 10–8 Ma) [e.g., *An et al*., 2001; *Allen and Armstrong*, 2012]. Therefore, we prefer an earlier onset of lower crustal flow than previously thought [*Clark et al*., 2005; *Schoenbohm et al*., 2006b]. Movement of lower crust would provide an important dragging force for upper crustal deformation, possibly initiating the Xianhuihe-Xiaojiang fault and causing the Ailao Shan-Red River fault, an inherited structure, to reactivate in the current kinematic regime with right-lateral strike slip [*Schoenbohm et al*., 2006b]. However, it may not have been the sole process in operation. Boundary stresses could also remain important driving forces. Lithospheric fragments continue to be extruded beyond the plateau through the late Cenozoic, but the rates of extrusion have become much slower [*Zhang et al*., 2004; *Royden et al*., 2008].

6. Conclusion

Our stratigraphic and structural observations indicate that the major bend in the Ailao Shan-Red River fault was a releasing bend in the early Miocene but became a restraining bend after the late Miocene reversal of displacement. Synthesis of our (U-Th)/He data and published geochronologic results show two phases of accelerated exhumation of the Ailao Shan Shear Zone, backed by stratigraphic and geomorphic observations. The first rapid exhumation phase occurred from ca. 27 to 17 Ma. Cover rocks were removed rapidly, and metamorphic rocks were exhumed to the near Earth's surface during this phase. The early Miocene sediments derived from Yangtze platform rocks within the shear zone were deposited in the releasing bend. This period of exhumation was followed by a tectonic quiescence during which a low-relief erosion surface was developed. The second episode of rapid exhumation began at 14–13 Ma, lasting 2–3 Myr. During this interval, the Ailao Shan range may have risen to its modern elevation, with high relief developing along the range due to river incision. Accordingly, metamorphic clasts from the shear zone continued to be deposited in the bend. Our results favor the injection of weak crustal material as a cause for the middle–late Miocene exhumation of the Ailao Shan Shear Zone and the reversal of displacement on the Red River fault. The coincidence of tectonic events in the Tibetan Plateau and its surroundings in the middle–late Miocene indicates possible dramatic dynamic change during the course of plateau growth.

Acknowledgments

All data used in this paper are published and available on demand to the corresponding author (geozhangbo@pku.edu.cn). This work is supported by National Natural Science Foundation of China (41272217 and 41422206) grant to Bo Zhang. We appreciate the Chinese Scholarship Council (CSC) for supporting Joint PhD student Project. We thank Fei Wang, Lin Wu, and $^{40}Ar/^{39}Ar$ and (U-Th)/He geochronology laboratory of Institute of Geology and Geophysics, Chinese Academy of Sciences, for analytical work. We acknowledge discussions with Zhaojie Guo, Zhicheng Zhang, and Barbara Carrapa. We sincerely thank Associate Editor Marc Jolivet, reviewer Anne Replumaz, and two anonymous reviewers for their thorough, critical, and constructive reviews. We also thank Editor Nathan Niemi for editorial handling and constructive comments.

References

Akciz, S., B. C. Burchfiel, J. L. Crowley, Y. Jiyun, and C. Liangzhong (2008), Geometry, kinematics, and regional significance of the Chong Shan shear zone, Eastern Himalayan Syntaxis, Yunnan, China, *Geosphere*, *4*(1), 292–314.

Allen, C. R., Y. Han, K. E. Sieh, B. Zhang, and C. N. Zhu (1984), Red River and associated faults, Yunnan Province, China: Quaternary geology, slip rate, and seismic hazard, *Geol. Soc. Am. Bull.*, *95*, 686–700.

Allen, C. R., Z. L. Luo, H. Qian, X. Z. Wen, H. W. Zhou, and W. S. Huang (1991), Field study of a highly active fault zone: The Xianshuihe fault of southwestern China, *Geol. Soc. Am. Bull.*, *103*, 1178–1199.

Allen, M. B., and H. A. Armstrong (2012), Reconciling the Intertropical Convergence Zone, Himalayan/Tibetan tectonics, and the onset of the Asian monsoon system, *J. Asian Earth Sci.*, *44*, 36–47.

An, Z., J. E. Kutzbach, W. L. Prell, and S. C. Porter (2001), Evolution of Asian monsoons and phased uplift of the Himalaya-Tibetan plateau since Late Miocene times, *Nature*, *411*(6833), 62–66.

Armijo, R., P. Tapponnier, and H. Tonglin (1989), Late Cenozoic right-lateral strike slip faulting in southern Tibet, *J. Geophys. Res.*, *94*, 2787–2838, doi:10.1029/JB094iB03p02787.

Ault, A. K., R. M. Flowers, and S. A. Bowring (2009), Phanerozoic burial and unroofing history of the western Slave craton and Wopmay orogen from apatite (U-Th)/He thermochronometry, *Earth Planet. Sci. Lett.*, *284*(1–2), 1–11.

Bai, D., et al. (2010), Crustal deformation of the eastern Tibetan plateau revealed by magnetotelluric imaging, *Nat. Geosci.*, *3*(5), 358–362.

Bergman, S. C., P. H. Leloup, P. Tapponnier, U. Schfirer, and P. O'Sullivan (1997), Apatite fission track thermal history of the Ailao Shan-Red River shear zone, China paper presented at meeting, Eur. Union of Geosci., Strasbourg France, 23–27 March.

Blisniuk, P. M., B. R. Hacker, J. Glodny, L. Ratschbacher, S. W. Bi, Z. H. Wu, M. O. McWilliams, and A. Calvert (2001), Normal faulting in central Tibet since at least 13.5 Myr ago, *Nature*, *412*(6847), 628–632.

Bovet, P. M., B. D. Ritts, G. Gehrels, A. O. Abbink, B. Darby, and J. Hourigan (2009), Evidence of Miocene crustal shortening in the north Qilian Shan from Cenozoic stratigraphy of the western Hexi Corridor, Gansu Province, China, *Am. J. Sci.*, *309*(4), 290–329.

Bureau of Geology and Mineral Resources of Yunnan Province (BGMR) (1990), *Regional Geology of Yunnan Province*, 728 pp., Geol. Publ. House, Beijing.

Cao, S., F. Neubauer, J. Liu, J. Genser, and B. Leiss, (2011), Exhumation of the Diancang Shan metamorphic complex along the Ailao Shan-Red River belt, southwestern Yunnan, China: Evidence from $^{40}Ar/^{39}Ar$ thermochronology, *J. Asian Earth Sci.*, *42*(3), 525–550.

Chen, W., P. H. Leloup, and M. Harrison (1993), $^{40}Ar/^{39}Ar$ results from the Ailao Shan and the Diancang Shan report, Univ. of Calif., Los Angeles, Calif.

Chen, X., J. Liu, Y. Tang, Z. Song, and S. Cao (2015), Contrasting exhumation histories along a crustal-scale strike-slip fault zone: The Eocene to Miocene Ailao Shan-Red River shear zone in southeastern Tibet, *J. Asian Earth Sci.*, *114*, 174–187.

Chung, S. L., T. Lee, C. Lo, P. Wang, C. Chen, N. Yem, T. Hoa, and W. Genyao (1997), Intraplate extension prior to continental extrusion along the Ailao Shan-Red River shear zone, *Geology*, *25*, 311–314.

Clark, M. K., M. A. House, L. H. Royden, K. X. Whipple, B. C. Burchfiel, X. Zhang, and W. Tang (2005), Late Cenozoic uplift of southeastern Tibet, *Geology*, *33*(6), 525–528.

Clark, M. K., L. H. Royden, K. X. Whipple, B. C. Burchfiel, X. Zhang, and W. Tang (2006), Use of a regional, relict landscape to measure vertical deformation of the eastern Tibetan Plateau, *J. Geophys. Res.*, *111*, F03002, doi:10.1029/2005JF000294.

Copley, A., and J. Jackson (2006), Active tectonics of the Turkish-Iranian Plateau, *Tectonics*, *25*, TC6006, doi:10.1029/2005TC001906.
Cunningham, W. D., and P. Mann (2007), Tectonics of strike-slip restraining and releasing bends, *Geol. Soc. London Spec. Publ.*, *290*(1), 1–12.
Duvall, A. R., M. K. Clark, E. Kirby, K. A. Farley, W. H. Craddock, C. Li, and D. Y. Yuan (2013), Low-temperature thermochronometry along the Kunlun and Haiyuan Faults, NE Tibetan Plateau: Evidence for kinematic change during late-stage orogenesis, *Tectonics*, *32*, 1190–1211, doi:10.1002/tect.20072.
Fang, X., D. Liu, C. Song, S. Dai, and Q. Meng (2013), Oligocene slow and Miocene-Quaternary rapid deformation and uplift of the Yumu Shan and North Qilian Shan: Evidence from high-resolution magnetostratigraphy and tectonosedimentology, *Geol. Soc. London Spec. Publ.*, *373*(1), 149–171.
Farley, K. A., R. A. Wolf, and L. T. Silver (1996), The effects of long alpha-stopping distances on (U-Th)/He ages, *Geochim. Cosmochim. Acta*, *60*(21), 4223–4229.
Farley, K. A. (2000), Helium diffusion from apatite: General behavior as illustrated by Durango fluorapatite, *J. Geophys. Res.*, *105*, 2903–2914, doi:10.1029/1999JB900348.
Flowers, R. M., R. A. Ketcham, D. L. Shuster, and K. A. Farley (2009), Apatite (U-Th)/He thermochronometry using a radiation damage accumulation and annealing model, *Geochim. Cosmochim. Acta*, *73*(8), 2347–2365.
Fyhn, M. B. W., and P. V. Phach (2015), Late Neogene structural inversion around the northern Gulf of Tonkin, Vietnam: Effects from right-lateral displacement across the Red River fault zone, *Tectonics*, *34*, 290–312, doi:10.1002/2014TC003674.
Gallagher, K. (2012), Transdimensional inverse thermal history modelling for quantitative thermochronology, *J. Geophys. Res.*, *117*, B02408, doi:10.1029/2011JB008825.
Gilley, L. D., T. M. Harrison, P. H. Leloup, F. J. Ryerson, O. M. Lovera, and J. H. Wang (2003), Direct dating of left-lateral deformation along the Red River shear zone, China and Vietnam, *J. Geophys. Res.*, *108*(B2), 2127, doi:10.1029/2001JB001726.
Godard, V., R. Pik, J. Lavé, R. Cattin, B. Tibari, J. De Sigoyer, M. Pubellier, and J. Zhu (2009), Late Cenozoic evolution of the central Longmen Shan, eastern Tibet: Insight from (U-Th)/He thermochronometry, *Tectonics*, *28*, TC5009, doi:10.1029/2008TC002407.
Guo, S., F. Ji, H. Xiang, X. Dong, F. Yan, S. Zhang, X. Li, and W. Zhang (2013), *Red River Active Fault Zone* [in Chinese], 172 pp., Ocean Press, Beijing.
Harrison, T. M., P. H. Leloup, F. J. Ryerson, P. Tapponnier, R. Lacassin, and W. J. Chen (1996), Diachronous initiation of transtension along the Ailao Shan-Red River shear zone, Yunnan and Vietnam, in *The Tectonic Evolution of Asia*, edited by A. Yin and T. M. Harrison, pp. 208–226, Cambridge Univ. Press, New York.
Hoke, G. D., J. Liu-Zeng, M. T. Hren, G. K. Wissink, and C. N. Garzione (2014), Stable isotopes reveal high southeast Tibetan Plateau margin since the Paleogene, *Earth Planet. Sci. Lett.*, *394*, 270–278.
Houseman, G., and P. England (1993), Crustal thickening versus lateral expulsion in the Indian-Asian continental collision, *J. Geophys. Res.*, *98*, 12,233–12,249, doi:10.1029/93JB00443.
Jolivet, M., M. Brunel, D. Seward, Z. Xu, J. Yang, F. Roger, P. Tapponnier, J. Malavieille, N. Arnaud, and C. Wu (2001), Mesozoic and Cenozoic tectonics of the northern edge of the Tibetan plateau: Fission-track constraints, *Tectonophysics*, *343*(1), 111–134.
Jolivet, M., F. Roger, Z. Q. Xu, J. L. Paquette, and H. Cao (2015), Mesozoic–Cenozoic evolution of the Danba dome (Songpan Garze, East Tibet) as inferred from LA-ICPMS U-Pb and fission-track data, *J. Asian Earth Sci.*, *102*, 180–204.
Ketcham, R. A. (2005), Forward and inverse modeling of low-temperature thermochronometry data, *Rev. Mineral. Geochem.*, *58*(1), 275–314.
Kirby, E., P. W. Reiners, M. A. Krol, K. X. Whipple, K. V. Hodges, K. A. Farley, W. Tang, and Z. Chen (2002), Late Cenozoic evolution of the eastern margin of the Tibetan Plateau: Inferences from $^{40}Ar/^{39}Ar$ and (U-Th)/He thermochronology, *Tectonics*, *21*(1), 1001, doi:10.1029/2000TC001246.
Lai, Q., L. Ding, H. Wang, Y. Yue, and F. Cai (2007), Constraining the stepwise migration of the eastern Tibetan Plateau margin by apatite fission track thermochronology, *Sci. China, Ser. D: Earth Sci.*, *50*(2), 172–183.
Lease, R. O., D. W. Burbank, M. K. Clark, K. A. Farley, D. Zheng, and H. Zhang (2011), Middle Miocene reorganization of deformation along the northeastern Tibetan Plateau, *Geology*, *39*(4), 359–362.
Lee, H. Y., et al. (2003), Miocene Jiali faulting and its implications for Tibetan tectonic evolution, *Earth Planet. Sci. Lett.*, *205*(3), 185–194.
Leloup, P. H., and J. R. Kienast (1993), High-temperature metamorphism in a major strike-slip shear zone: The Ailao Shan-Red River, People's Republic of China, *Earth Planet. Sci. Lett.*, *118*, 213–234.
Leloup, P. H., R. Lacassin, P. Tapponnier, U. Schärer, D. L. Zhong, X. H. Liu, L. S. Zhang, S. C. Ji, and T. T. Phan (1995), The Ailao Shan-Red River shear zone (Yunnan, China), Tertiary transform boundary of Indochina, *Tectonophysics*, *251*, 3–84.
Leloup, P. H., N. Arnaud, R. Lacassin, J. R. Kienast, T. M. Harrison, T. T. Phan Trong, A. Replumaz, and P. Tapponnier (2001), New constraints on the structure, thermochronology, and timing of the Ailao Shan-Red River shear zone, SE Asia, *J. Geophys. Res.*, *106*, 6683–6732, doi:10.1029/2000JB900322.
Li, S., B. S. Currie, D. B. Rowley, and M. Ingalls (2015), Cenozoic paleoaltimetry of the SE margin of the Tibetan Plateau: Constraints on the tectonic evolution of the region, *Earth Planet. Sci. Lett.*, *432*, 415–424.
Liu, J., Y. Tang, M. D. Tran, S. Cao, L. Zhao, Z. Zhang, and W. Chen (2012), The nature of the Ailao Shan-Red River (ASRR) shear zone: Constraints from structural, microstructural and fabric analyses of metamorphic rocks from the Diancang Shan, Ailao Shan and Day Nui Con Voi massifs, *J. Asian Earth Sci.*, *47*, 231–251.
Liu-Zeng, J., P. Tapponnier, Y. Gaudemer, and L. Ding (2008), Quantifying landscape differences across the Tibetan Plateau: Implications for topographic relief evolution, *J. Geophys. Res.*, *113*, F04018, doi:10.1029/2007JF000897.
McDowell, F. W., W. C. McIntosh, and K. A. Farley (2005), A precise ^{40}Ar-^{39}Ar reference age for the Durango apatite (U-Th)/He and fission-track dating standard, *Chem. Geol.*, *214*, 249–263.
Molnar, P., and J. M. Stock (2009), Slowing of India's convergence with Eurasia since 20 Ma and its implications for Tibetan mantle dynamics, *Tectonics*, *28*, TC3001, doi:10.1029/2008TC002271.
Molnar, P., and P. Tapponnier (1975), Cenozoic tectonics of Asia: Effects of a continental collision, *Science*, *189*(4201), 419–426.
Nelson, K. D., et al. (1996), Partially molten middle crust beneath southern Tibet: Synthesis of project indepth results, *Science*, *274*(5293), 1684–1688.
Ouimet, W., K. Whipple, L. Royden, P. Reiners, K. Hodges, and M. Pringle (2010), Regional incision of the eastern margin of the Tibetan Plateau, *Lithosphere*, *2*(1), 50–63.
Reid, A. J., A. P. Fowler, D. Phillips, J. Christopher, and C. J. Wilson (2005), Thermochronology of the Yidun Arc, central eastern Tibetan Plateau: Constraints from $^{40}Ar/^{39}Ar$ K-feldspar and apatite fission track data, *J. Asian Earth Sci.*, *25*(6), 915–935.
Replumaz, A., R. Lacassin, P. Tapponnier, and P. H. Leloup (2001), Large river offsets and Plio-Quaternary dextral slip rate on the Red River fault (Yunnan, China), *J. Geophys. Res.*, *106*, 819–836, doi:10.1029/2000JB900135.
Roger, F., S. Calassou, J. Lancelot, J. Malavieille, M. Mattauer, Z. Xu, Z. Hao, and L. Haou (1995), Miocene emplacement and deformation of the Konga Shan granite (Xianshui He fault zone, west Sichuan, China): Geodynamic implications, *Earth Planet. Sci. Lett.*, *130*, 201–216.
Royden, L. H., B. C. Burchfiel, R. W. King, E. Wang, Z. Chen, F. Shen, and Y. Liu (1997), Surface deformation and lower crustal flow in Eastern Tibet, *Science*, *276*(5313), 788–790.
Royden, L. H., B. C. Burchfiel, and R. D. van der Hilst (2008), The geological evolution of the Tibetan Plateau, *Science*, *321*(5892), 1054–1058.

Schoenbohm, L., K. Whipple, and B. C. Burchfiel (2004), River incision into a relict landscape along the Ailao Shan shear zone and Red River fault in Yunnan Province, China, *Geol. Soc. Am. Bull.*, *116*, 895–909.
Schoenbohm, L., B. C. Burchfiel, L. Chen, and J. Yin (2005), Exhumation of the Ailao Shan shear zone recorded by Cenozoic sedimentary rocks, Yunnan Province, China, *Tectonics*, *24*, TC6015, doi:10.1029/2005TC001803.
Schoenbohm, L., B. C. Burchfiel, L. Chen, and J. Yin (2006a), Miocene to present activity along the Red River fault, China, in the context of continental extrusion, upper crustal rotation, and lower crustal flow, *Geol. Soc. Am. Bull.*, *118*, 672–688.
Schoenbohm, L., B. C. Burchfiel, and L. Chen (2006b), Propagation of surface uplift, lower crustal flow, and Cenozoic tectonics of the southeast margin of the Tibetan Plateau, *Geology*, *34*(10), 813–816.
Searle, M. P., M. W. Yeh, T. H. Lin, and S. L. Chung (2010), Structural constraints on the timing of left-lateral shear along the Red River shear zone in the Ailao Shan and Diancang Shan Ranges, Yunnan, SW China, *Geosphere*, *6*(4), 316–338.
Shen, J., Y. P. Wang, and F. M. Song (2003), Characteristics of the active Xiaojiang fault zone in Yunnan, China: A slip boundary for the southeastward escaping Sichuan-Yunnan Block of the Tibetan Plateau, *J. Asian Earth Sci.*, *21*(10), 1085–1096.
Shen, Z. K., J. Lü, M. Wang, and R. Bürgmann (2005), Contemporary crustal deformation around the southeast borderland of the Tibetan Plateau, *J. Geophys. Res.*, *110*, B11409, doi:10.1029/2004JB003421.
Sonder, L. J., P. C. England, B. P. Wernicke, and R. L. Christiansen (1987), A physical model for Cenozoic extension of western North America, *Geol. Soc. London Spec. Publ.*, *28*, 187–201.
Tapponnier, P., G. Peltzer, A. Y. Le Dain, R. Armijo, and P. Cobbold (1982), Propagating extrusion tectonics in Asia: New insights from simple experiments with plasticine, *Geology*, *10*, 611–616.
Tapponnier, P., R. Lacassin, P. H. Leloup, U. Schärer, D. Zhong, X. Liu, S. Ji, L. Zhang, and J. Zhong (1990), The Ailao Shan-Red River metamorphic belt: Tertiary left-lateral shear between Indochina and south China, *Nature*, *343*, 431–437.
Tapponnier, P., Z. Q. Xu, F. Roger, B. Meyer, N. Arnaud, G. Wittlinger, and J. S. Yang (2001), Geology: Oblique stepwise rise and growth of the Tibet Plateau, *Science*, *294*, 1671–1677.
Tian, Y., B. P. Kohn, A. J. W. Gleadow, and S. Hu (2014), A thermochronological perspective on the morphotectonic evolution of the southeastern Tibetan Plateau, *J. Geophys. Res. Solid Earth*, *119*, 676–698, doi:10.1002/2013JB010429.
Wang, E., B. C. Burchfiel, L. H. Royden, L. Z. Chen, J. S. Chen, W. X. Li, and L. Chen (1998), *Late Cenozoic Xianshuihe-Xiaojiang, Red River, and Dali Fault Systems of Southwestern Sichuan and Central Yunnan*, GSA Bookstore, China.
Wang, E., E. Kirby, K. P. Furlong, M. Van Soest, G. Xu, X. Shi, P. J. J. Kamp, and K. V. Hodges (2012), Two-phase growth of high topography in eastern Tibet during the Cenozoic, *Nat. Geosci.*, *5*(9), 640–645.
Wang, G., J. Wan, E. Wang, D. Zheng, and F. Li (2008), Late Cenozoic to recent transtensional deformation across the Southern part of the Gaoligong shear zone between the Indian plate and SE margin of the Tibetan plateau and its tectonic origin, *Tectonophysics*, *460*(1), 1–20.
Wang, P. L., C. H. Lo, T. Y. Lee, S. L. Chung, C. Y. Lan, and N. T. Yem (1998), Thermochronological evidence for the movement of the Ailao Shan-Red River shear zone: A perspective from Vietnam, *Geology*, *26*(10), 887–890.
Wang, S., X. M. Fang, D. W. Zheng, and E. C. Wang (2009), Initiation of slip along the Xianshuihe fault zone, eastern Tibet, constrained by K/Ar and fission-track ages, *Int. Geol. Rev.*, *51*(12), 1121–1131.
Wang, S., J. Guiguo, X. Tiande, T. Yuntao, Z. Dewen, and F. Xiaomin (2012), The Jinhe-Qinghe fault—An inactive branch of the Xianshuihe-Xiaojiang fault zone, *Eastern Tibet, Tectonophysics*, *544–545*, 93–102.
Wang, Y., B. Zhang, J. Hou, and X. Xu (2014), Structure and tectonic geomorphology of the Qujiang fault at the intersection of the Ailao Shan-Red River fault and the Xianshuihe-Xiaojiang fault system, China, *Tectonophysics*, *634*, 156–170.
Williams, H., S. Turner, S. Kelley, and N. Harris (2001), Age and composition of dikes in Southern Tibet: New constraints on the timing of east-west extension and its relationship to postcollisional volcanism, *Geology*, *29*(4), 339–342.
Wu, L., P. Monié, F. Wang, W. Lin, W. Ji, M. Bonno, P. Münch, and Q. Wang (2016), Cenozoic exhumation history of Sulu terrane: Implications from (U–Th)/He thermochrology, *Tectonophysics*, *672*, 1–15.
Xiang, H. F., L. Wan, Z. Han, S. Guo, W. Zhang, L. Chen, and L. Dong (2006), Initiation of large-scale dextral strike-slip movement of Red River fault by Fission Track ages, *Sci. China, Ser. D: Earth Sci.*, *36*(11), 977–987.
Xiang, H. F., S. Guo, W. Zhang, Z. Jun, B. Zhang, J. Wan, X. Dong, and L. Chen (2007), Quantitative study on the large scale dextral strike-slip offset in the southern segment of the Red River fault since Miocene [in Chinese with English abstract], *Seismol. Geol.*, *29*(1), 34–50.
Xu, G., and P. Kamp (2000), Tectonics and denudation adjacent to the Xianshuihe Fault, eastern Tibetan Plateau: Constraints from fission track thermochronology, *J. Geophys. Res.*, *105*, 19,231–19,251, doi:10.1029/2000JB900159.
Xu, X. W., and Q. D. Deng (1996), Nonlinear characteristics of paleoseismicity in China, *J. Geophys. Res.*, *101*, 6209–6231, doi:10.1029/95JB01238.
Yang, R., M. G. Fellin, F. Herman, S. D. Willett, W. Wang, and C. Maden (2016), Spatial and temporal pattern of erosion in the Three Rivers Region, southeastern Tibet, *Earth Planet. Sci. Lett.*, *433*, 10–20.
Yin, A. (2010), Cenozoic tectonic evolution of Asia, a preliminary synthesis, *Tectonophysics*, *488*, 293–325.
Yin, A., and T. M. Harrison (2000), Geologic evolution of the Himalayan-Tibetan Orogen, *Annu. Rev. Earth Planet. Sci.*, *28*, 211–280.
Yuan, D. Y., J. D. Champagnac, W. P. Ge, P. Molnar, P. Z. Zhang, W. J. Zheng, H. P. Zhang, and X. W. Liu (2011), Late Quaternary right-lateral slip rates of faults adjacent to the lake Qinghai, northeastern margin of the Tibetan Plateau, *Geol. Soc. Am. Bull.*, *123*(9–10), 2016–2030.
Yuan, W., J. Dong, W. Shicheng, and A. Carter (2006), Apatite fission track evidence for Neogene uplift in the eastern Kunlun Mountains, north Qinghai-Tibet Plateau, China, *J. Asian Earth Sci.*, *27*, 847–856.
Zhang, B., J. Zhang, D. Zhong, L. Yang, Y. Yue, and S. Yan (2012), Polystage deformation of the Gaoligong metamorphic zone: Structures, $^{40}Ar/^{39}Ar$ mica ages, and tectonic implications, *J. Struct. Geol.*, *37*, 1–18.
Zhang, H., W. H. Craddock, R. O. Lease, W. Wang, D. Y. Yuan, P. Z. Zhang, P. Molnar, D. W. Zheng, and W. J. Zheng (2012), Magnetostratigraphy of the Neogene Chaka basin and its implications for mountain building processes in the north-eastern Tibetan Plateau, *Basin Res.*, doi:10.1111/j.1365-2117.2011.00512.x.
Zhang, H., M. E. Oskin, J. Liu-Zeng, P. Zhang, P. W. Reiners, and P. Xiao (2016), Pulsed exhumation of interior eastern Tibet: Implications for relief generation mechanisms and the origin of high-elevation planation surfaces, *Earth Planet. Sci. Lett.*, *449*, 176–185.
Zhang, J., D. Zhong, H. Sang, and Y. Zhou (2006), Structural and geochronological evidence for multiple episodes of deformation since Paleocene along the Ailao Shan-Red River shear zone, southeastern Asia [in Chinese with English abstract], *Chin. J. Geol.*, *41*(2), 291–310.
Zhang, P. Z., et al. (2004), Continuous deformation of the Tibetan Plateau from Global Positioning System data, *Geology*, *32*(9), 809–812.
Zhang, Y. Z., A. Replumaz, G. C. Wang, P. H. Leloup, C. Gautheron, M. Bernet, P. Beek, J. L. Paquette, A. Wang, and K. Zhang (2015), Timing and rate of exhumation along the Litang fault system, implication for fault reorganization in Southeast Tibet, *Tectonics*, *34*, 1219–1243, doi:10.1002/2014TC003671.
Zheng, D., M. K. Clark, P. Zhang, W. Zheng, and K. A. Farley (2010), Erosion, fault initiation and topographic growth of the North Qilian Shan (northern Tibetan Plateau), *Geosphere*, *6*(6), 937–941.